

Resonant Higgs boson pair production in the $hh \rightarrow b\bar{b} WW \rightarrow b\bar{b}\ell^+\nu\ell^-\bar{\nu}$ decay channel

Víctor Martín Lozano,^{a,b} Jesús M. Moreno^a and Chan Beom Park^{c,d}

^a*Instituto de Física Teórica, IFT-UAM/CSIC, Nicolás Cabrera 13,
UAM Cantoblanco, 28049 Madrid, Spain.*

^b*Dept. Física Teórica, Universidad Autónoma de Madrid, 28049 Madrid, Spain.*

^c*Korea Institute for Advanced Study, Seoul 130-722, Korea.*

^d*CERN, Theory Division, 1211 Geneva 23, Switzerland.*

E-mail: victor.martinlozano@uam.es, jesus.moreno@csic.es,
cbpark@kias.re.kr

ABSTRACT: Adding a scalar singlet provides one of the simplest extensions of the Standard Model. In this work we briefly review the latest constraints on the mass and mixing of the new Higgs boson and study its production and decay at the LHC. We mainly focus on double Higgs production in the $hh \rightarrow b\bar{b}WW \rightarrow b\bar{b}\ell^+\nu\ell^-\bar{\nu}$ decay channel. This decay is found to be efficient in a region of masses of the heavy Higgs boson of 260 – 500 GeV, so it is complementary to the $4b$ channel, more efficient for Higgs bosons having masses greater than 500 GeV. We analyse this di-leptonic decay channel in detail using kinematic variables such as M_{T2} and the M_{T2} -assisted on-shell reconstruction of invisible momenta. Using proper cuts, a significance of $\sim 3\sigma$ for 3000 fb^{-1} can be achieved at the 14 TeV LHC for $m_H = 260 - 400 \text{ GeV}$ if the mixing is close to its present limit and $\text{BR}(H \rightarrow hh) \approx 1$. Smaller mixing values would require combining various decay channels in order to reach a similar significance. The complementarity among $H \rightarrow hh$, $H \rightarrow ZZ$ and $H \rightarrow WW$ channels is studied for arbitrary $\text{BR}(H \rightarrow hh)$ values.

KEYWORDS: Higgs physics, Beyond Standard Model, Hadron-Hadron Scattering, Particle and resonance production

Contents

1	Introduction	1
2	The singlet-extended model	2
3	Constraints on m_H and $\sin \alpha$	3
4	Detecting the heavy Higgs in $H \rightarrow hh$ at the LHC	6
5	Comments on Dark Matter	24
5.1	Relic density	25
5.2	Direct Detection	25
6	Conclusions	27
A	Higgs M_{T2} in di-leptonic WW process	28

1 Introduction

The discovery at the LHC by ATLAS and CMS collaborations of a scalar boson compatible with the Standard Model (SM) Higgs boson [1, 2] has opened a new era in particle physics. Since there are several Higgs production modes and five of its decay processes have been measured ($\gamma\gamma$, ZZ^* , WW^* , $\tau\bar{\tau}$, and $b\bar{b}$), it is possible to extract its couplings and compare with SM predictions. A useful variable to evaluate the consistency of the experimental data with the SM Higgs hypothesis is the so-called signal-strength modifier defined as $\hat{\mu} = \sigma_{\text{observed}}/\sigma_{\text{SM}}$ for each channel. In the latest analyses of the full 7 and 8 TeV LHC data, ATLAS [3] and CMS [4] obtained following combined values

$$\begin{aligned}\hat{\mu}_{\text{ATLAS}} &= 1.30^{+0.18}_{-0.17} \quad (m_h = 125.36 \text{ GeV}), \\ \hat{\mu}_{\text{CMS}} &= 1.00 \pm 0.13 \quad (m_h = 125.02 \text{ GeV})\end{aligned}\tag{1.1}$$

from the main Higgs production and decay modes. If we ignore the small difference in the m_h value used in the two fits¹ and assume that there are no correlation and gaussian error, the combined value is given by²

$$\hat{\mu}_{\text{ATLAS+CMS}} = 1.10 \pm 0.10.\tag{1.2}$$

¹Both m_h and $\hat{\mu}$ should be fitted simultaneously.

²For a recent analysis including Tevatron data and taking into account the correlation among the different measurements, see [5].

Thus, the experimental data is certainly consistent with the SM predictions and it can be used to constrain new physics.

The simplest modification to the Higgs couplings is given by a generic rescaling of them and this would be the case in the minimal extension of the Higgs sector, in which a scalar singlet that generically mixes with the ordinary SM Higgs is included. This is the model that we will analyze in this work. Adding a singlet to the SM scalar sector has implications that have been widely explored in the literature. It can help to stabilize the Higgs potential at high energies through their positive contributions to renormalization group equations that govern the Higgs quartic coupling evolution [6]. It can rescue the electroweak baryogenesis scenario by providing a strong enough first-order electroweak phase transition, as studied in refs. [7, 8] (see however, ref. [9]). Moreover, it can act as a dark matter (DM) candidate [10] or as a portal to DM [11–14], depending on its stability.

If the new scalar is not too heavy, it can be produced at the LHC through the mixing with the ordinary Higgs and detected by the conventional heavy SM-like Higgs boson searches [15–20]. On the other hand, if the double-Higgs decay mode is open, it will decrease the significance of SM-like Higgs signatures. Consequently, it is important to explore the specific resonant double-Higgs production [21–25]. In this work we extend previous analysis, focusing on the particular $hh \rightarrow b\bar{b}WW \rightarrow b\bar{b}\ell^+\nu\ell^-\bar{\nu}$ process, and present strategies to enhance the signal-background ratio by using various kinematic variables.

The organization of our paper is as follows. In Section 2 we briefly describe the model. Then, we review the present constraints on the mass of the new singlet and its mixing in Section 3. In turn, we study the production of the heavy scalar and explore its detection in the next LHC run using the double-Higgs decay channel with $b\bar{b}\ell^+\nu\ell^-\bar{\nu}$ as a final state. We comment on the complementarity of this channel and the decays into two electroweak gauge bosons. The interplay between direct production and indirect effects, such as the modification of the Higgs couplings, will be considered for a luminosity of 3000 fb^{-1} in Section 4. In the next section we check the validity of our study when extending the model to accommodate for a DM candidate. Finally, we present the conclusions.

2 The singlet-extended model

One of the simplest extension of the SM Higgs sector is given by the addition of a real singlet field. This model has been also widely studied in refs. [21, 22, 24, 26–44]. The relevant Lagrangian for the scalar sector is as follows:

$$\mathcal{L} = (D_\mu \Phi)^\dagger (D^\mu \Phi) + \frac{1}{2} \partial_\mu S \partial^\mu S - V(\Phi, S), \quad (2.1)$$

with the potential [21, 29]

$$\begin{aligned} V(\Phi, S) = & \lambda_{40} \left(\Phi^\dagger \Phi - v^2 \right)^2 + \lambda_{21} v \left(\Phi^\dagger \Phi - v^2 \right) S + \lambda_{22} \left(\Phi^\dagger \Phi - v^2 \right) S^2 \\ & + \lambda_{02} v^2 S^2 + \lambda_{03} v S^3 + \lambda_{04} S^4. \end{aligned} \quad (2.2)$$

The physical doublet and singlet scalar fields can be obtained by expanding the scalar potential $V(\Phi, S)$ around the real neutral vacuum expectation values (VEVs):

$$\Phi = \begin{pmatrix} 0 \\ v + \phi/\sqrt{2} \end{pmatrix}, \quad S = v_S + s. \quad (2.3)$$

We take $v \simeq 174$ GeV and have chosen $V(\Phi, S)$ such that $v_S = 0$.³ The conditions $\lambda_{40} > 0$, $\lambda_{04} > 0$, and $\lambda_{22} > -2\sqrt{\lambda_{40}\lambda_{04}}$ have to be imposed in order to ensure that the potential is bounded from below.

Due to the λ_{21} term, the two scalars ϕ and s mix and the mass eigenstates are given by

$$\begin{pmatrix} h \\ H \end{pmatrix} = \begin{pmatrix} \cos \alpha & \sin \alpha \\ -\sin \alpha & \cos \alpha \end{pmatrix} \begin{pmatrix} \phi \\ s \end{pmatrix}. \quad (2.4)$$

The mixing angle α and the mass eigenvalues read

$$\begin{aligned} \tan 2\alpha &= \frac{\lambda_{21}\sqrt{2}}{2\lambda_{02} - \lambda_{40}} \\ m_{H,h}^2 &= \left(2\lambda_{40} + \lambda_{02} \pm \sqrt{2\lambda_{21}^2 + (2\lambda_{40} - \lambda_{02})^2} \right) v^2. \end{aligned} \quad (2.5)$$

The stability of the vacuum requires $\lambda_{02} > 0$ and $4\lambda_{40}\lambda_{02} > \lambda_{21}^2$. We can use (2.5) to express $(\lambda_{40}, \lambda_{02}, \lambda_{21})$ in terms of the physical parameters α , m_h , m_H , and v as follows:

$$\begin{aligned} \lambda_{40} &= \frac{m_h^2 \sin^2 \alpha + m_H^2 \cos^2 \alpha}{8v^2}, \\ \lambda_{02} &= \frac{m_h^2 \cos^2 \alpha + m_H^2 \sin^2 \alpha}{4v^2}, \\ \lambda_{21} &= \frac{(m_H^2 - m_h^2) \sin 2\alpha}{2\sqrt{2}v^2}. \end{aligned} \quad (2.6)$$

The cubic and quartic interactions involving the mass eigenstates h , H can be given as functions of the physical parameters (2.5) and the three remaining couplings $(\lambda_{22}, \lambda_{03}, \lambda_{04})$. This is in contrast with the SM (or in the extended complex Higgs singlet model), where the full potential can be reconstructed from the mass (matrix) and the VEVs of the field(s). In what follows, we assume that h , the lighter Higgs, is the SM-like Higgs discovered at the LHC having $m_h \sim 125$ GeV. Its couplings approach the SM ones in the $\cos \alpha \approx 1$ limit.

3 Constraints on m_H and $\sin \alpha$

The deviation of the Higgs couplings from their SM values is constrained by the LHC Higgs data and by the electroweak precision observables (EWPO). We first concentrate on the latter. The Higgs contributes to the gauge bosons self-energies involved in the EWPO. In

³Note that, in a generic potential, S can be shifted to fulfill this condition.

the singlet-extended Higgs model, the one loop self-energies will be given by the sum of two SM-like Higgs contributions evaluated at Higgs masses, m_h and m_H , rescaled by $\cos^2 \alpha$ and $\sin^2 \alpha$ respectively [21]. This property can also be applied to non-universal diagrams (*e.g.*, vertex corrections) involving the Higgses and it is transmitted to the EWPO in the limit where higher order, $\mathcal{O}(\sin^4 \alpha)$ terms, are neglected. Taking this into account and using ZFITTER [45–52], we have evaluated the predictions for the Z -peak observables [53] and m_W , Γ_W [54], as a function of m_H and $\sin^2 \alpha$. The list of observables used are listed in Table 1. The results are presented in Figure 1, where 90% and 95% C.L. allowed regions

Observable	Data	Observable	Data
m_W	80.385 ± 0.015	$\sin^2 \theta_{\text{eff}}^\ell$	0.2324 ± 0.0012
Γ_W	2.085 ± 0.042	A_c	0.670 ± 0.027
Γ_Z	2.4952 ± 0.0023	A_b	0.923 ± 0.020
σ_{had}^0	41.540 ± 0.037	$A_{\text{FB}}^{0,c}$	0.0707 ± 0.0035
R_ℓ^0	20.767 ± 0.025	$A_{\text{FB}}^{0,b}$	0.0992 ± 0.0016
$A_{\text{FB}}^{0,\ell}$	0.0171 ± 0.0010	R_c^0	0.1721 ± 0.0030
A_ℓ	0.1499 ± 0.0018	R_b^0	0.21629 ± 0.00066

Table 1. Electroweak data taken from ref. [55] used in the fit of the EWPO.

in the $m_H - \sin^2 \alpha$ plane are shown. The structure of these lines can be understood by noting that at $m_H = m_h$ the contour line is a vertical one since its value does not depend on the mixing angle. On the other hand, for large m_H values, the mixing angle must be small enough to compensate the non-decoupling Higgs contributions to the EWPO.

It is also common to use the oblique parameters (S , T , U) instead of analyzing the complete set of observables. We expect that in the region where $m_H \lesssim 200$ GeV both methods should give a similar χ^2 value. However, for larger m_H values, the gaussian approximation to the χ^2 that is used to fit (S , T , U) and the estimation of their errors starts to break down.⁴ This can be explicitly checked by evaluating χ^2 as a function of m_h using the whole Z -peak data or the oblique parameters (S , T , U).

Let us now consider the impact of the LHC Higgs data. As already mentioned in the introduction, the reduction of the Higgs couplings to SM fields due to the mixing translates into a common reduction of the Higgs signal-strength modifier in all channels. By applying the narrow-width approximation, one can see that this factor is given by $\cos^2 \alpha$. Using eq. (1.2), it is straightforward to derive the following bound on the mixing: $\sin^2 \alpha < 0.076$ (0.128) at 90% (95%) C.L. We can now combine this bound with the ones derived from the EWPO: the results are given in Figure 2.

After dealing with the indirect bounds⁵ on the mixing for a given m_H value, we briefly comment on the direct ones, derived from heavy Higgs boson searches. Note that, as a

⁴This is shown in [56], where a detailed calculation of Δr and m_W in the singlet-extended model is presented.

⁵There are other constraints that can be derived by imposing perturbative unitarity of scattering amplitudes for longitudinal W bosons [38, 57]. We will ignore them since they are weaker than the other bounds [11].

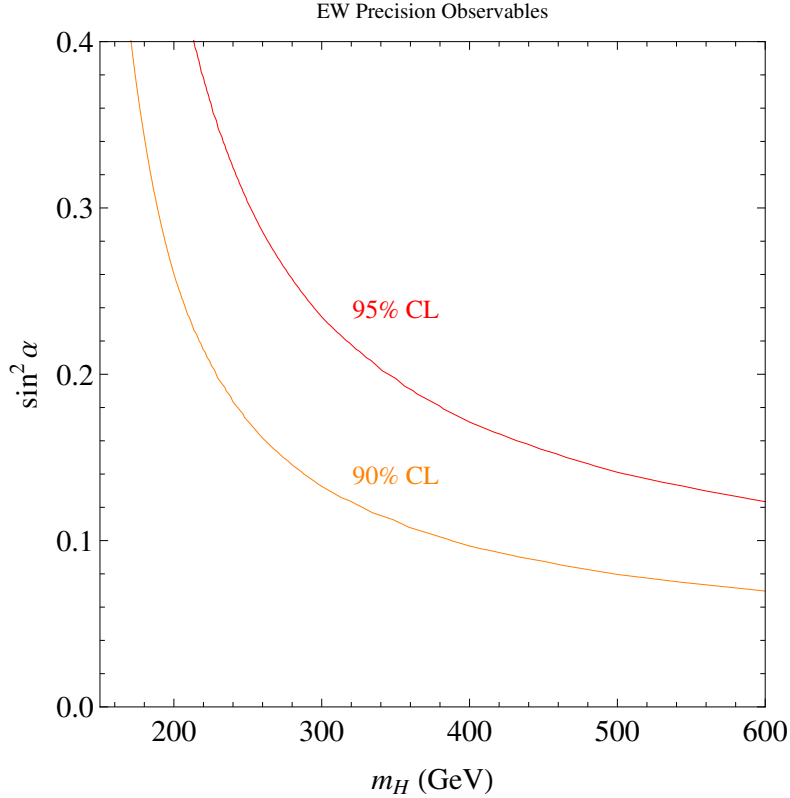


Figure 1. Constraints in the $m_H - \sin^2 \alpha$ derived from the full set of EWPO at the Z -peak.

consequence of the mixing, the production and decay modes of the singlet-like Higgs H will be the same as those of the SM-like Higgs. However, as it has different mass, the branching ratios of the decay channels will be different from the SM-like Higgs. We can reinterpret ATLAS and CMS analyses for heavy Higgs searches to derive bounds on m_H and $\sin^2 \alpha$. The ATLAS collaboration presented two searches for the heavy Higgs boson. The first one uses $H \rightarrow WW \rightarrow \ell\nu\ell\nu$ [15] decay mode and the bound corresponds to an integrated luminosity of 21 fb^{-1} at $\sqrt{s} = 8 \text{ TeV}$. The second one uses the $H \rightarrow ZZ$ decay [17]. The CMS collaboration has reported two analyses on heavy Higgs searches using the $H \rightarrow ZZ$ decay channels. The first one corresponds to integrated luminosity 19.6 fb^{-1} at $\sqrt{s} = 8 \text{ TeV}$ and considers the $\ell^+\ell^-q\bar{q}$ final state [18]. The second one considers final states where both Z 's decay into charged leptons and corresponds to integrated luminosity 5.1 fb^{-1} at $\sqrt{s} = 7 \text{ TeV}$ and 19.6 fb^{-1} at $\sqrt{s} = 8 \text{ TeV}$ [19]. The CMS collaboration has also performed an analysis using the channel $H \rightarrow WW \rightarrow \ell\nu\ell\nu$, obtained for the configurations of $\sqrt{s} = 7 \text{ TeV}$ with integrated luminosity of 4.9 fb^{-1} and $\sqrt{s} = 8 \text{ TeV}$ with 19.5 fb^{-1} [20]. The results are shown in Figure 3, where we have assumed that H has the same branching ratios as a SM Higgs would have for those masses. This is certainly a good approximation if the $H \rightarrow hh$ decay process is not kinematically allowed, or $\text{BR}(H \rightarrow hh) \ll 1$. On the other hand, if $\text{BR}(H \rightarrow hh)$ is substantially large, these bounds have to be rescaled as indicated

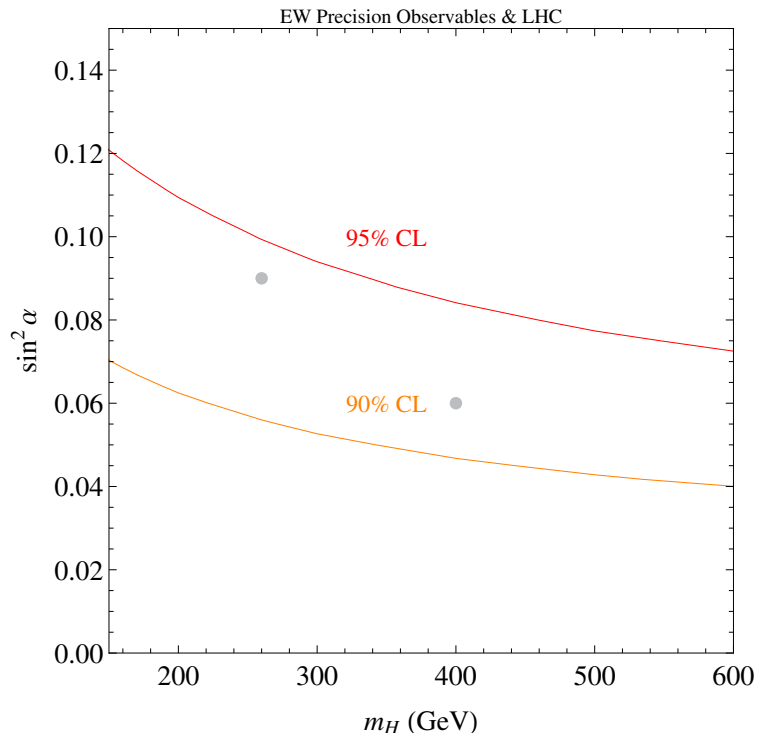


Figure 2. Constraints in the $m_H - \sin^2 \alpha$ plane derived from the full set of EWPO at the Z -peak combined with the LHC Higgs coupling data. We have also drawn the two benchmark points whose LHC implications are analyzed in detail in Section 4.

in the figure, and eventually will become irrelevant in the $\text{BR}(H \rightarrow hh) \sim 1$ limit. In this case, the double-Higgs production process will be the main signature of the model at the LHC and deserves a detailed study. We investigate the scenario in the next section, and in turn, present the interplay among the different, present and future, bounds.

4 Detecting the heavy Higgs in $H \rightarrow hh$ at the LHC

The resonant double Higgs production is a distinct feature of the model we are dealing with. In this section we study this process in the forthcoming LHC run at 14 TeV. Since the Higgs production cross-section $\sigma(H)$ scales as $\sin^2 \alpha$ and there is a bound on the allowed mixing for a given m_H , we can obtain the maximal value of $\sigma(H)$ as a function m_H . This is shown in Figure 4, where the 95% C.L. limit on $\sin^2 \alpha$ has been used.

In order to check the signal significance at the LHC, which will be resumed with the upgraded center-of-mass energy along the year 2015, we perform a Monte Carlo (MC) study by choosing two benchmark points. For the $H \rightarrow hh$ decay process, the largest portion of signal events will consist of the four- b -jet final state as studied in refs. [58, 59]. However, the multi-jet signature is generically vulnerable to the huge QCD backgrounds and the poor reconstruction efficiency. One can attempt to increase the purity of signal

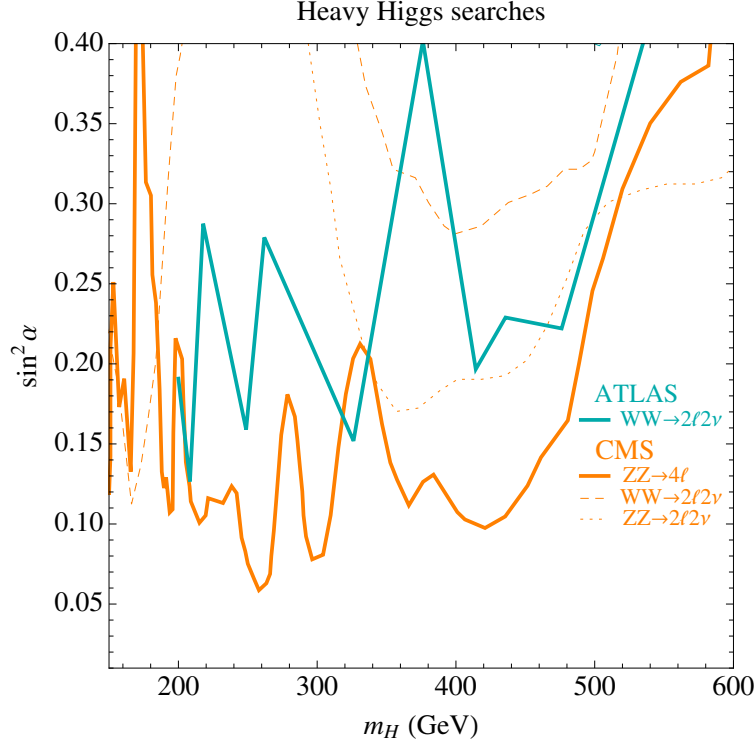


Figure 3. Constraints in the $m_H - \sin^2 \alpha$ plane derived by ATLAS and CMS from SM-like heavy Higgs searches assuming the heavy Higgs decays as the SM one. For non-zero $\text{BR}(H \rightarrow hh)$ values, the vertical axis would read $\sin^2 \alpha / (1 - \text{BR}(H \rightarrow hh))$.

events by imposing a tight b -tagging condition, but then it would result in a big sacrifice of the signal statistics. The ATLAS and CMS collaborations have performed searches for resonant double-Higgs production in the $b\bar{b}b\bar{b}$ final state [60, 61]. It was shown that in order to be effective in this channel the mass of the new resonance should be greater than 500 GeV to ensure two highly boosted, back-to-back $b\bar{b}$ di-jet systems [58]. For smaller masses, the acceptance times the efficiency of the search decreases, thus making difficult to use this channel.

The subleading decay process is $b\bar{b}W^+W^-$, followed by fully-hadronic, semi-leptonic, and di-leptonic modes. This search channel, as it will be shown below, can be efficient in the range of the heavy Higgs mass 260 – 500 GeV.⁶ Among them, the final states containing the lepton are more suitable for the search since the fully-hadronic states are liable to be in trouble due to the similar reason as in the four- b -jet signal. In leptonic signal events the missing energy originated from the neutrino prevents the direct reconstruction of the Higgs resonances. Still, provided that the light Higgs boson mass m_h is accurately known, one can obtain the neutrino four-momenta up to a two-fold ambiguity by using on-shell mass

⁶The complementary channel to the one presented here is the $b\bar{b}\gamma\gamma$ [62, 63]. The small branching ratio of the SM Higgs decaying into two photons makes this channel challenging (see, however refs. [64, 65]).

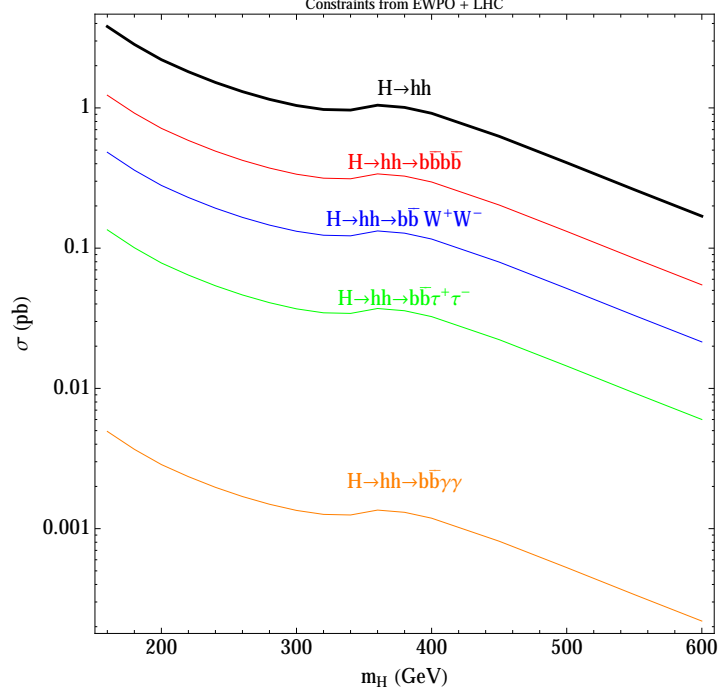


Figure 4. Cross-section of the double Higgs production mediated by the heavy Higgs boson evaluated at the maximal mixing angle. The black line shows the total cross section for this process while different final state cross sections are presented in colours.

relations as well as the missing energy condition in the case of the semi-leptonic channel:

$$(p^\nu)^2 = 0, \quad \left(p^\nu + p^\ell + p^q + p^{q'}\right)^2 = m_h^2, \quad \mathbf{p}_T^\nu = \mathbf{p}_T, \quad (4.1)$$

where \mathbf{p}_T is the missing transverse momenta measured in the event, and q and q' are jets from the hadronically-decaying W boson. On the other hand, the on-shell relations are not enough to constrain the neutrino momenta in the case of the di-leptonic channel even though it provides cleaner signal than the semi-leptonic one. We here examine the discovery potential of the di-leptonic decay mode, which appears to be more challengeable due to the missing neutrinos although it is less vulnerable to uncertainties regarding the jet reconstruction, by using various kinematic variables and an approximate reconstruction scheme. We will see the practicability and the limitation of the search strategy in two different scenarios characterized by

1. $m_H = 400$ GeV, $\sin^2 \alpha = 0.06$,
2. $m_H = 260$ GeV, $\sin^2 \alpha = 0.09$,

and assume $\text{BR}(H \rightarrow hh) = 1$ for both benchmark points.⁷

⁷We stress that the results obtained here can be readily reinterpreted for the scenario with different $\text{BR}(H \rightarrow hh)$ values.

The production cross-section is $\sigma(gg \rightarrow H) \times \text{BR}(H \rightarrow hh) = \sigma(gg \rightarrow \phi) \times \sin^2 \alpha \simeq 0.7$ (1.2) pb for $m_H = 400$ (260) GeV in the 14-TeV LHC condition. Here, ϕ is the Higgs-like scalar and $\sigma(gg \rightarrow \phi)$ values have been obtained from the Higgs Cross Section Working Group in [66] assuming that the couplings of ϕ are SM-like. The search channel of interest is

$$H \rightarrow hh \rightarrow b\bar{b}W^+W^- \rightarrow b(p^b)\bar{b}(p^{\bar{b}}) + \ell^+(p^\ell)\ell^-(q^\ell) + \cancel{E}_T \quad (\ell = e, \mu), \quad (4.2)$$

where the source of the missing energy is the neutrinos produced by the leptonically-decaying W bosons. For a numerical analysis, we have generated the MC events using PYTHIA 8 [67], interfacing with the CT10 parton distribution functions [68] for a proton-proton collision at $\sqrt{s} = 14$ TeV. The parton showering and the hadronization have been performed by PYTHIA 8. Then, the hadron-level data has been processed with the fast detector-simulation program DELPHES 3 [69], which reconstructs the final-state objects such as jets, isolated leptons, and the missing energy with the inclusion of detector resolution effects and tagging/fake rates. The input parameters have been adjusted for the ATLAS detector in DELPHES. FASTJET 3 [70] is employed to reconstruct jets. In our simulation, the anti- k_t jet algorithm [71] with distance parameter of 0.5 is chosen for the jet reconstruction. It is known that the tagging efficiency for the b -jet depends on the transverse momentum p_T and the pseudorapidity η of the jet object. Recent ATLAS and CMS analyses on the b -jet identification for the experimental data indicate that the efficiency can be as large as $\sim 60 - 80\%$ [72]. For the sake of a simple analysis, we assume a flat b -tagging efficiency of 70% for $p_T > 30$ GeV and $|\eta| < 2.5$ and the mis-tagging efficiency is set to be 10% for the c -jet and 1% for the light flavor as well as the gluon jet. Isolated electrons (muons) are required to have $p_T > 13$ (10) GeV within $|\eta| < 2.4$. In order to remove fake leptons coming from the decays of hadrons, we discard the leptons lying within the angular separation $\Delta R_{\ell j} = \sqrt{\Delta\phi_{\ell j}^2 + \Delta\eta_{\ell j}^2} < 0.4$ from a jet with $p_T > 25$ GeV. Since the tau reconstruction efficiency is relatively poor, we reject the events containing the tau-jet with $p_T > 10$ GeV. The missing transverse momentum \cancel{p}_T is defined as the opposite of the vector sum of all the visible particles' transverse momenta.

Having the same final states that the signal, the di-leptonic $t\bar{t}$ process is the main background. The subleading backgrounds include Drell-Yan (DY), di-boson, and the SM Higgs processes that lead into the leptonic final states and the b -jets. In addition, we consider the rare SM Higgs processes including the double-Higgs production via the gluon-gluon fusion (GGF), the single-Higgs production via the vector-boson fusion (VBF), and the Higgs boson produced in association with a weak vector boson or a top-pair, *i.e.*, hW/Z and $ht\bar{t}$. The SM double-Higgs events have been generated by a modified PYTHIA 6 program [73] in which the matrix element calculated with HPAIR [74] is implemented, while the other processes have been generated by PYTHIA 8. We use the production cross section for the SM double-Higgs process obtained by HPAIR, which can calculate up to a next-to-leading order value. The $t\bar{t}$ production cross section is calculated with TOP++ 1.4 [75] at next-to-next-leading order, and the Higgs production cross sections except that of the double-Higgs process are obtained from ref. [66]. For the DY and the di-boson

Process	Cross section
$H \rightarrow hh$ ($m_H = 400$ GeV)	0.66
$H \rightarrow hh$ ($m_H = 260$ GeV)	1.18
$t\bar{t}$	844.43
GGF h	50.35
VBF h	4.17
hW/Z	2.39
$ht\bar{t}$	0.61
hh	0.033
DY	91130.0
Di-boson	121.0

Table 2. Production cross sections in pb for the signal and background processes at the 14 TeV proton-proton collision. We set $m_t = 173.5$ GeV and $m_h = 125$ GeV.

processes, we use the leading-order cross sections calculated with PYTHIA 8 since most of them can contribute to the background by faking b -jets and can be readily removed by event selection cuts, which will be discussed shortly. In Table 2, we show the cross-section values used in this study.

Before going further into the analysis, we introduce one of the main kinematic variables and the reconstruction scheme adopted to obtain the approximate values of the invisible neutrino momenta. The situation with more than one invisible particle in a collider event is common in many extensions of the SM providing a viable DM candidate. One of the most studied collider variables to search for such a new physics signature is M_{T2} , which is a generalized transverse mass particularly known to be useful for the pair-production processes of new particles that eventually decay into the invisible particles [76, 77]. Suppose that the decay topology is like

$$pp \rightarrow Y + \bar{Y} + U \rightarrow V(p)\chi(k) + \bar{V}(q)\chi(l) + U(u), \quad (4.3)$$

where Y is a heavy unstable particle, V is a set of detectable particles such as jets or charged leptons, and χ is the invisible particle. Here, U denotes a set of particles that does not participate in the decay process of Y like initial or final state radiations. For the new physics signature with the decay topology (4.3), the invisible momenta k and l as well as the particle masses m_Y and m_χ are unknown, while only the sum of their transverse components can be inferred from the deficit of total transverse momentum in the collider

event, *i.e.*, the missing transverse momentum. Then, M_{T2} is defined as

$$M_{T2} \equiv \min_{\mathbf{k}_T + \mathbf{l}_T = \mathbf{p}_T} \left[\max \left\{ M_T^{(1)}, M_T^{(2)} \right\} \right], \quad (4.4)$$

where $M_T^{(i)}$ ($i = 1, 2$) are transverse masses for the decay chains,

$$\begin{aligned} \left(M_T^{(1)} \right)^2 &= m_V^2 + m_\chi^2 + 2 \left(\sqrt{|\mathbf{p}_T|^2 + m_V^2} \sqrt{|\mathbf{k}_T|^2 + m_\chi^2} - \mathbf{p}_T \cdot \mathbf{k}_T \right), \\ \left(M_T^{(2)} \right)^2 &= m_V^2 + m_\chi^2 + 2 \left(\sqrt{|\mathbf{q}_T|^2 + m_V^2} \sqrt{|\mathbf{l}_T|^2 + m_\chi^2} - \mathbf{q}_T \cdot \mathbf{l}_T \right). \end{aligned} \quad (4.5)$$

Here, \mathbf{k}_T , \mathbf{l}_T , and m_χ are input parameters. In practice, the transverse momenta of invisible particles are uniquely determined by the minimization, whereas the invisible particle mass m_χ is a constant that must be put by hand before the minimization. Once the correct m_χ value is chosen, the endpoint position of the M_{T2} distribution points to the parent particle mass,

$$M_{T2}(m_\chi = m_\chi^{\text{true}}) \leq m_Y. \quad (4.6)$$

The situation becomes simpler when the invisible particle mass is already known as in the case of SM processes, where the neutrino is the only particle escaping detection and can be safely assumed to be massless for reconstruction purposes.⁸ Another notable feature of the M_{T2} variable is that it comes in handy even when one or both parent particles are off-shell. This has been studied to measure the SM Higgs boson mass in the di-leptonic $WW^{(*)}$ channel [82, 83]. In the case when $m_h < 2m_W$, at least one of the W bosons should be produced off-shell. Then, the maximal value of M_{T2} is not m_W , but $\sim m_h/2$. This can be deduced by considering some special kinematic configurations as derived in Appendix A.

As mentioned above, the di-leptonic system cannot be solved by on-shell mass relations even if Higgs boson masses are known. However, there is an approximation scheme to solve the unknown neutrino momenta by help of M_{T2} . When the minimization has been finalized to obtain the M_{T2} value, a unique solution for the transverse momentum configuration is picked up. One may attempt to see the correlation between these hypothetical momentum components and the true ones. For a subset of events whose M_{T2} values are close to M_{T2}^{max} , it can be shown that the M_{T2} solution of the transverse momenta are very close or equal to the true momenta. This can be justified by the fact that the M_{T2} solution is unique while preserving kinematic constraints,⁹ and the endpoint of the transverse mass corresponds to the invariant mass of the decaying system, *i.e.*, the parent particle mass. Then, by adopting the M_{T2} solution of the invisible transverse momenta in conjunction with known on-shell mass relations, one can calculate the longitudinal and energy components of the invisible

⁸The application of M_{T2} to the SM di-leptonic $t\bar{t}$ process was firstly proposed in [78]. It is later employed and checked its efficiency in the real experimental analyses measuring the top quark mass at both Tevatron and the LHC [79–81].

⁹ The $M_T^{(i)}$ ($i = 1, 2$) functions are ellipses in the phase space and the M_{T2} value is determined by their intersecting point in the balanced configuration. This feature can be used to seek the M_{T2} value by using a sophisticated algorithm proposed in [84].

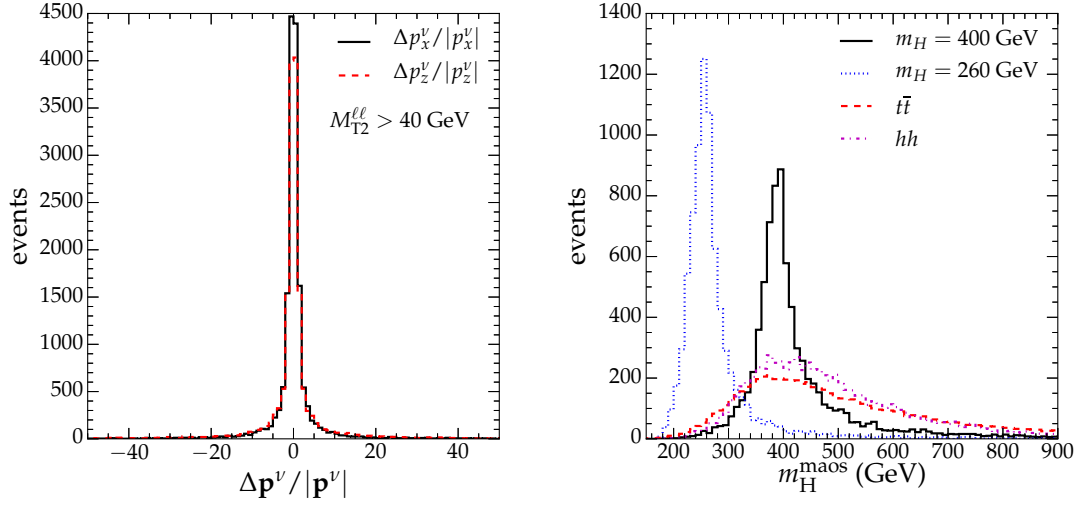


Figure 5. (Left panel) Difference between the MAOS momentum and the true neutrino momentum for $m_H = 400$ GeV $\Delta \mathbf{p}^\nu/|\mathbf{p}^\nu| \equiv (\mathbf{p}_\nu^{\text{maos}} - \mathbf{p}_\nu^{\text{true}})/|\mathbf{p}_\nu^{\text{true}}|$. (Right panel) Normalized m_H^{maos} distributions for $m_H = 260$ and 400 GeV and the $t\bar{t}$ backgrounds using parton-level data.

four-momenta. This is so-called M_{T2} -assisted on-shell (MAOS) approximation scheme [85]. One drawback of this scheme is that it cannot be applied if any of the parent particles are off-shell. However, it was claimed that one can circumvent the on-shell mass problem by substituting the transverse mass for the decay chain instead of the invariant mass into the on-shell mass relation [82, 83, 86]. It means that the on-shell mass relations now become

$$(p + k^{\text{maos}})^2 = \left(M_T^{(1)}\right)^2, \quad (q + l^{\text{maos}})^2 = \left(M_T^{(2)}\right)^2. \quad (4.7)$$

This modified scheme guarantees that there is always a real solution for the invisible momenta since the transverse mass is bounded from above by the invariant mass, and it maintains the property that the MAOS momentum is equal to the true momentum for the endpoint events of M_{T2} . See the left panel of Figure 5, where the efficiency of approximation to the invisible momenta in the modified scheme is shown. Since the light Higgs boson mass here is set to be $125 \text{ GeV} < 2m_W$, one or both W bosons produced by the Higgs boson are always off-shell. In this situation, the modified MAOS scheme (4.7) can be applied. Once the MAOS momentum has been obtained, one can construct the invariant mass of the total system, which corresponds to the heavy singlet-like Higgs boson mass given by

$$(m_H^{\text{maos}})^2 \equiv \left(p^b + p^{\bar{b}} + p^\ell + q^\ell + k^{\text{maos}} + l^{\text{maos}}\right)^2 \simeq m_H^2. \quad (4.8)$$

Strictly speaking, the equality holds only when $k^{\text{maos}} = k^{\text{true}}$ and $l^{\text{maos}} = l^{\text{true}}$. The right panel of Figure 5, which shows m_H^{maos} distributions for the heavy Higgs signal and the SM double-Higgs as well as $t\bar{t}$ backgrounds using the parton-level MC event samples. One can

see that the peak position of the signal distribution clearly matches the m_H value, while broad distributions are exhibited in the non-resonant background process.

Armed with these tools, we now discuss our analysis to search for the heavy Higgs signal. After reconstructing the final-state objects, we select events that passed the basic cuts given as follows.

- At least two isolated, opposite-sign leptons including the electron or the muon, *i.e.*, $e^\pm e^\mp$, $\mu^\pm \mu^\mp$, and $e^\pm \mu^\mp$. We further require that one of them must have $p_T > 20$ GeV,
- At least two b -tagged jets with $p_T > 30$ GeV,
- Missing energy $\cancel{E}_T > 20$ GeV,
- For the opposite-sign same-flavor leptons, the event is rejected if $m_{\ell+\ell^-} < 12$ GeV to avoid the leptons produced by decays of the hadrons, and the Z -veto condition, which discards events containing $|m_{\ell+\ell^-} - m_Z| < 15$ GeV, is imposed.

We note that all the cut values have been chosen to optimize the signal significance. In the signal events, all the leptons are produced in the $h \rightarrow WW^*$ decay process. In this case, it is known that the spin correlations of the decay mode make the charged leptons collinear. This feature can be used to further reduce the leptonic backgrounds. We use two angular cuts: the azimuthal angular difference $|\Delta\phi_{\ell\ell}| < 1.32$ (1.57) and $\Delta R_{\ell\ell} \equiv \sqrt{(\Delta\phi_{\ell\ell})^2 + (\Delta\eta_{\ell\ell})^2} < 1.34$ (1.58) for the Higgs signal with $m_H = 400$ (260) GeV. The upper frames in Figure 6 show clear separation between the signal and the $t\bar{t}$ background, particularly when $m_H = 400$ GeV. This is because the leptons can be much more boosted in the heavier Higgs events. The collinearity of leptons is also encoded in the other cut variables, the sum of the transverse momenta $p_T^{\ell\ell} = |\mathbf{p}_T^\ell + \mathbf{q}_T^\ell|$ and the di-lepton invariant mass $m_{\ell\ell}$. In the case when $m_H = 260$ GeV, the leptons are less energetic so that the $p_T^{\ell\ell}$ is relatively soft. See the lower frames in Figure 6. We require that $p_T^{\ell\ell} > 42$ (25) GeV and $m_{\ell\ell} < 60$ (47) GeV for the $m_H = 400$ (260) GeV scenarios. The $m_{\ell\ell}$ cut can also remove the $Z \rightarrow \tau^+ \tau^-$ events in which the tau leptons decay leptonically.

In addition to the basic selection and the leptonic cuts, one can impose cuts on the b -jets. Recently, a boosted Higgs technique has been developed for processes like $pp \rightarrow hV$ ($V = W, Z$) [87] or $pp \rightarrow hh$ [88], followed by $h \rightarrow b\bar{b}$. In the situation where the Higgs boson is substantially boosted, the jets produced by the Higgs boson can often be considered as one fat jet, whose mass is around m_h . For very high $p_T^h \gg m_h$, $\Delta R_{bb} \equiv \sqrt{(\Delta\phi_{bb})^2 + (\Delta\eta_{bb})^2}$ can be estimated to be

$$\Delta R_{bb} \simeq \frac{2m_h}{p_T^h}. \quad (4.9)$$

If the fat Higgs jet condition could be applied, the backgrounds, in particular, the $t\bar{t}$ events would be reduced very efficiently since the b -jets in the background can have a relatively

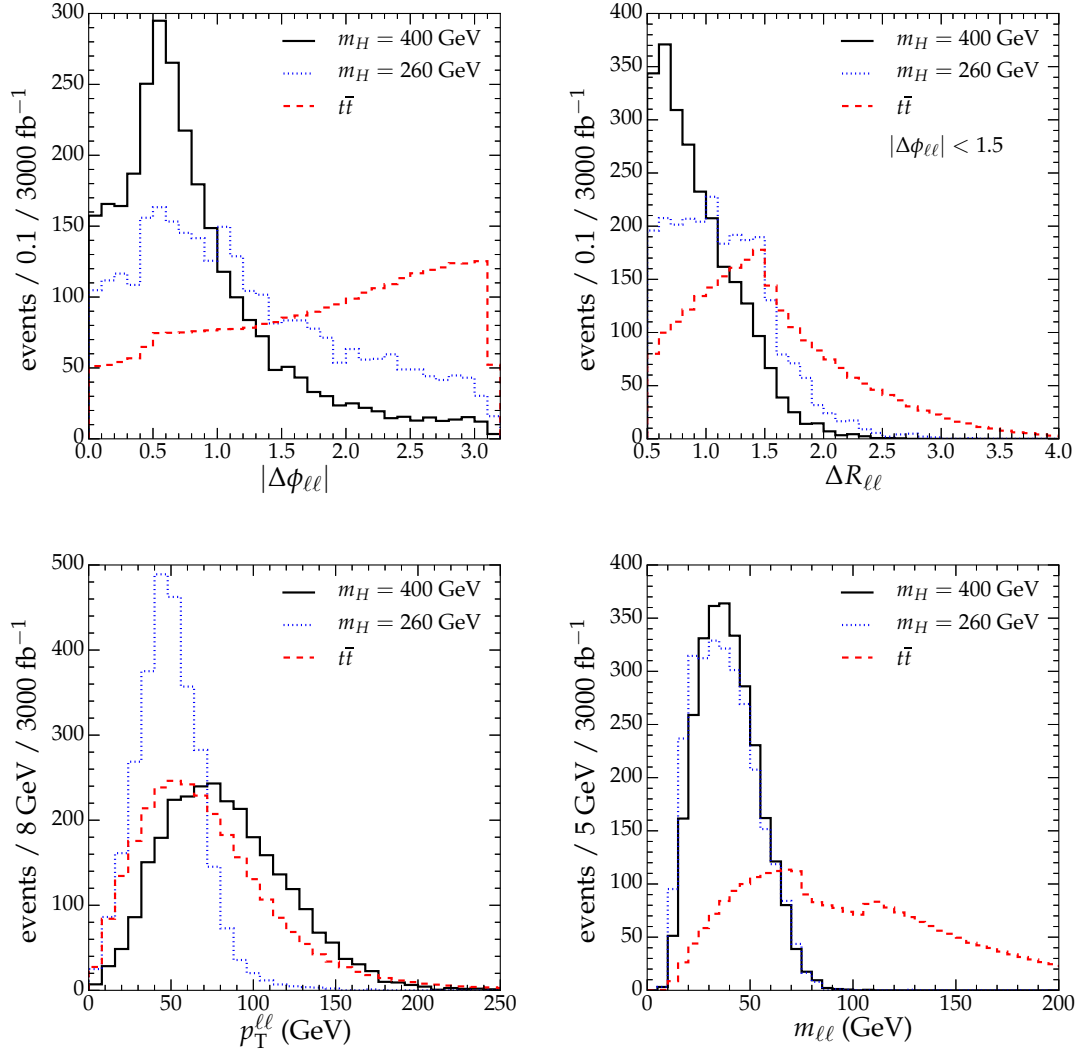


Figure 6. Detector-level distributions of the kinematic variables for the two charged leptons. The upper frames are (Left panel) the azimuthal angular separations and (Right panel) the $\Delta R_{\ell\ell}$ when applying the azimuthal angular cut has been imposed. The lower frames are (Left panel) the sum of transverse momenta $p_T^{\ell\ell}$ and (Right panel) the invariant mass $m_{\ell\ell}$ distributions. Basic selection cuts are applied and all the distributions are normalized for an illustration.

large angular separation. In the Higgs signal, p_T^h can be as large as

$$p_T^h = \frac{m_H}{2} \sqrt{1 - \frac{4m_h^2}{m_H^2}} \simeq 156 \text{ GeV}. \quad (4.10)$$

so $\Delta R_{bb} \simeq 1.6$ for $m_H = 400$ GeV in the rest frame of the heavy Higgs boson. The left panel in the upper frames of Figure 7 justifies this estimation. Normally, the fat Higgs jet is required to have $\Delta R_{bb} \sim 1.2 - 1.5$ or $p_T^h \gtrsim 200$ GeV. Provided that the heavy Higgs boson is produced at near-threshold energy, the transverse momentum of the light Higgs has an

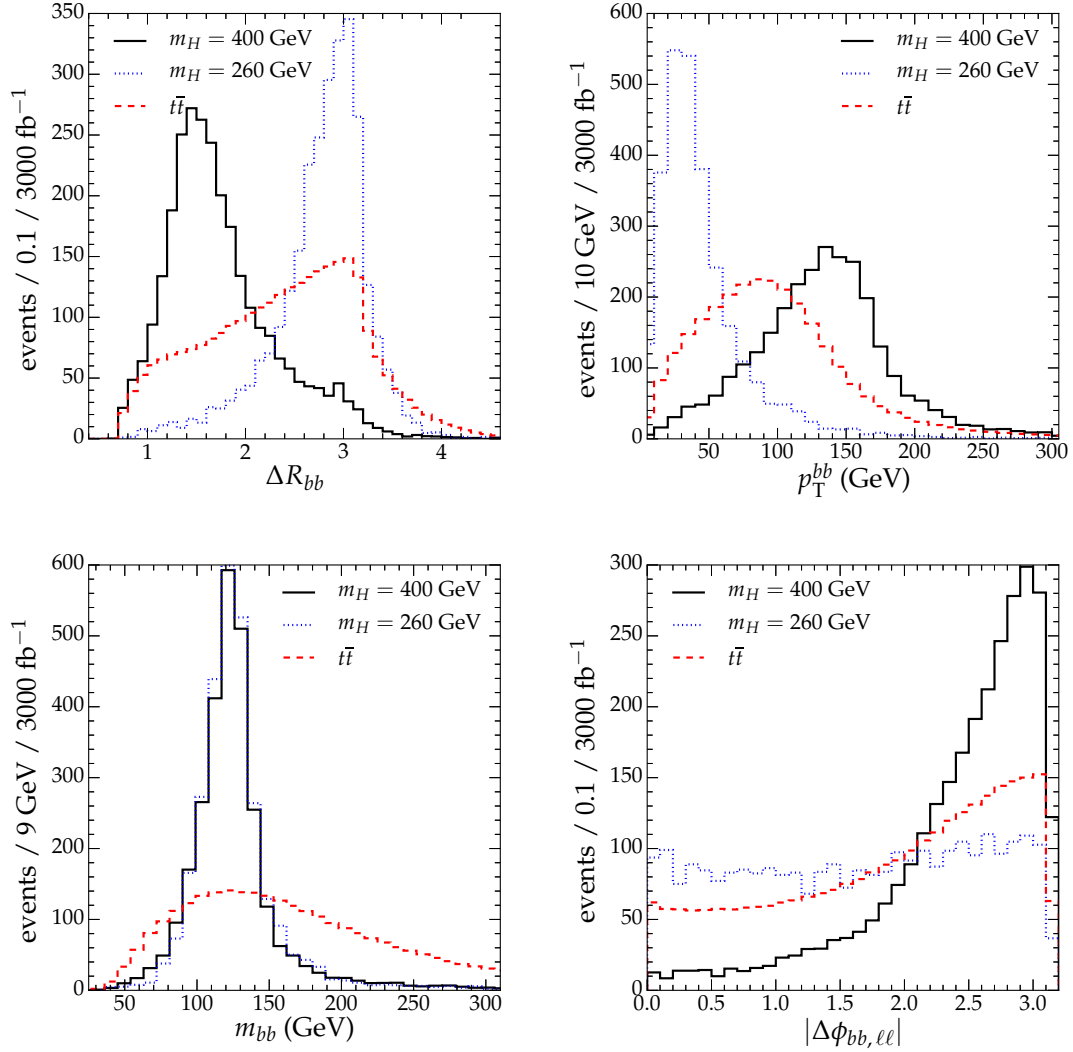


Figure 7. Detector-level distributions of the kinematic variables for the two b -tagged jets. The upper frames are (Left panel) ΔR_{bb} and (Right panel) the transverse momentum p_T^{bb} . The lower frames are (Left panel) the di- b -jet invariant mass and (Right panel) the azimuthal angular separation between $b\bar{b}$ and $\ell^+\ell^-$ systems. Basic selection cuts are applied and all the distributions are normalized for an illustration.

upper bound as given in (4.10). Therefore, we expect that the boosted Higgs technique will be applicable in the case of much heavier Higgs boson with $m_H \gtrsim 490$ GeV.

In our benchmark points, it is inevitable to use the conventional kinematic cuts. Although the angular separations of the b -jets are rather sizable, it still turns out to be smaller than the backgrounds in the case when $m_H = 400$ GeV, while the cut can be applied in the opposite way in the case when $m_H = 260$ GeV. This can be easily deduced from eq. (4.9), which predicts that the angular separation can be very large for the smaller p_T^b value. On

the other hand, the right panel in the upper frames of Figure 7 shows that $m_H = 400$ GeV signal events possess much larger values of the total transverse momentum for the $b\bar{b}$ system. We select events with $\Delta R_{bb} < 2.25$ and $p_T^{bb} > 105$ GeV for $m_H = 400$ GeV, while $\Delta R_{bb} > 2.56$ without imposing any p_T^{bb} cut for $m_H = 260$ GeV signal events. Since the m_h value is already known, one can further impose a cut on the di- b -jet invariant mass to ensure that the b -jets are originated from the light Higgs boson. One can see that the invariant mass distributions have clear peaks around $m_h = 125$ GeV for both benchmark points in the left panel in the lower frames of Figure 7. The invariant mass is required to have a value within a mass window of 115 (94) GeV $< m_{bb} < 146$ (135) GeV for $m_H = 400$ (260) GeV signal.

In the case when the heavy Higgs boson is produced near threshold, the light Higgs boson pair will be almost in a back-to-back configuration. Then, it is likely that the direction of the $b\bar{b}$ system will be well separated from that of the $\ell^+\ell^-$ system. This feature can be seen in the right panel in the lower frames of Figure 7, where the distributions for the absolute value of $\Delta\phi_{bb,\ell\ell} \equiv \cos^{-1}(\hat{\mathbf{p}}_T^{bb} \cdot \hat{\mathbf{p}}_T^{\ell\ell})$, where $\hat{\mathbf{p}}_T \equiv \mathbf{p}_T/p_T$, are shown. We take events with $|\Delta\phi_{bb,\ell\ell}| > 1.92$ for $m_H = 400$ GeV signal. This cut is not applicable to the case of the $m_H = 260$ GeV signal as the angular separation can be relatively small due to the small boost of each Higgs decay chain.

We now turn to the M_{T2} cuts. For the $2b + 2\ell + \cancel{E}_T$ final state, one can construct two kinds of M_{T2} according to the definition for the visible + invisible system, that is, either $2\ell + \cancel{E}_T$, which contains leptons only, or $2b + 2\ell + \cancel{E}_T$, which contains b -jets as well as leptons when forming the visible particle system. We emphasize that M_{T2} has been known to be applicable to a system that can be divided into two groups of visible particles like processes depicted in the decay topology (4.3) with a pair production of heavy particles, followed by two separate decay chains. The $2\ell + \cancel{E}_T$ system in the signal decay topology (4.2) can be regarded as such a process. In what follows, the M_{T2} calculated for the $2\ell + \cancel{E}_T$ system is expressed as $M_{T2}^{\ell\ell}$ to distinguish it from the other kind of M_{T2} . As is derived in Appendix A for some kinematic configurations, the $M_{T2}^{\ell\ell}$ distribution is bounded from above by $m_h/2 < m_W$, whereas it has a maximum at m_W in the di-leptonic $t\bar{t}$ process since both W bosons are in on-shell. The $M_{T2}^{\ell\ell}$ distributions in the left panel of Figure 8 clearly show the endpoint structure. Another notable feature is that there are a number of events which have vanishing $M_{T2}^{\ell\ell}$ for both signal and background distributions. It corresponds to a trivial zero of $M_{T2}^{\ell\ell}$ in the fully massless case, *i.e.*, $m_\ell = m_\nu = 0$ [89]. This happens when the missing transverse momentum $\cancel{\mathbf{p}}_T$ lies on the smaller sector of the transverse plane spanned by the visible momentum vectors \mathbf{p}_T^ℓ and \mathbf{q}_T^ℓ . In this case, the $M_{T2}^{\ell\ell}$ value is taken for a momentum partition where both transverse masses in eqs. (4.5) are vanishing. However, the fraction of events with the trivial zero of the $M_{T2}^{\ell\ell}$ can be different depending on the preferred momentum configuration of the process. Due to the spin correlation and the boost, the opening angle of the charged leptons in the Higgs signal event is smaller than that in the di-leptonic $t\bar{t}$ events as was seen in the upper frames of Figure 6. It means that there are more chances to have the trivial zero of $M_{T2}^{\ell\ell}$ in the $t\bar{t}$ events than in the Higgs signal. Therefore, the lower cut as well as the upper one can help

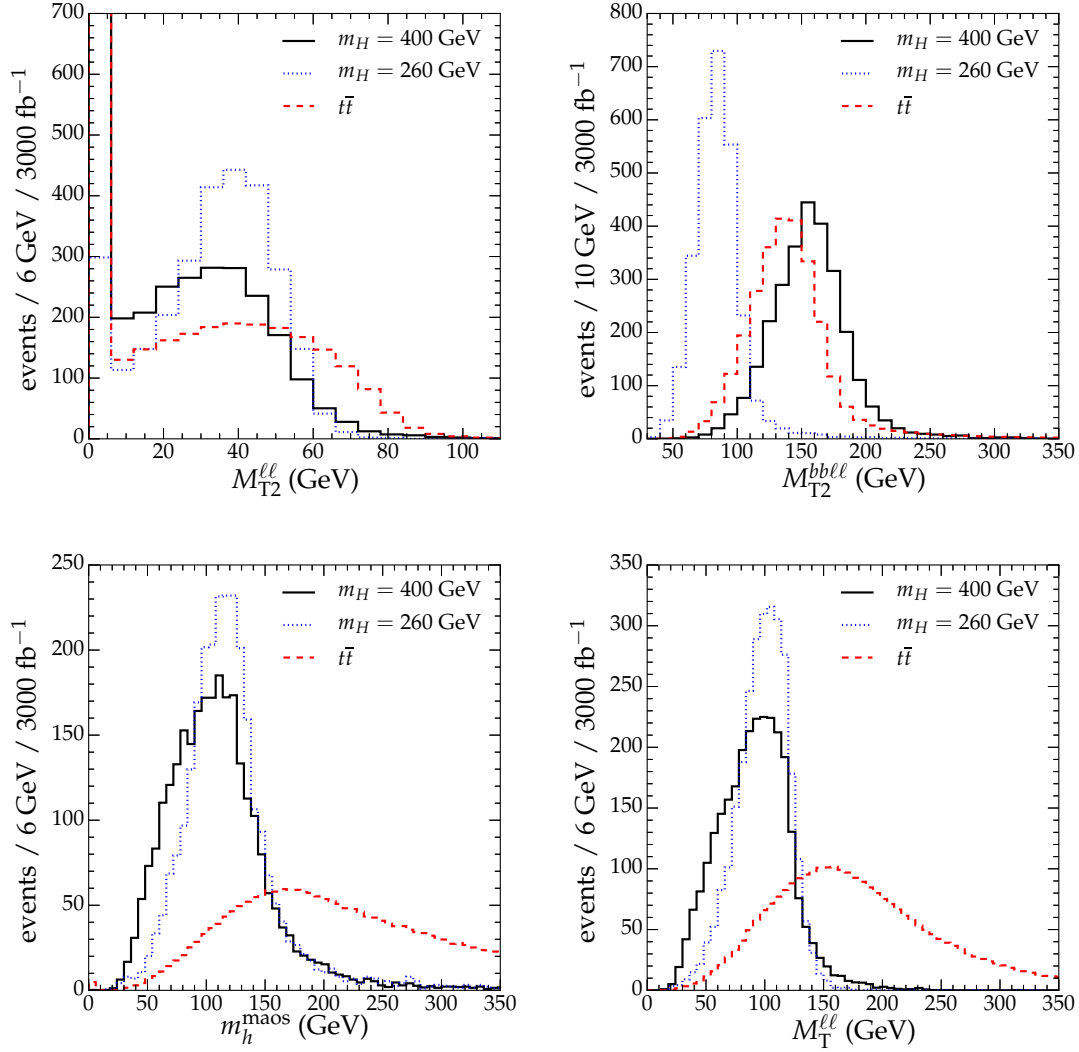


Figure 8. The upper frames are detector-level M_{T2} distributions for (Left panel) the $2\ell + \cancel{E}_T$ and (Right panel) $2b + 2\ell + \cancel{E}_T$ systems. The lower frame are (Left panel) m_h^{maos} and (Right panel) $M_T^{\ell\ell}$ distributions for detector-level signals and backgrounds. Basic selection cuts are applied and all the distributions are normalized for an illustration.

reduce the backgrounds further. This lower cut on the $M_{T2}^{\ell\ell}$ also increases the accuracy of the MAOS momenta, which will be used in the subsequent analysis. We impose the $M_{T2}^{\ell\ell}$ cut as $25 \text{ GeV} < M_{T2}^{\ell\ell} < 60 \text{ GeV}$ for $m_H = 260 \text{ GeV}$ signal. In the case when $m_H = 400 \text{ GeV}$, the missing transverse momentum vector can lie inside of the opening angle of the di-lepton system when the light Higgs is fairly boosted. Therefore, we do not apply the lower cut, but only the upper cut $M_{T2}^{\ell\ell} < 60 \text{ GeV}$ is imposed for the $m_H = 400 \text{ GeV}$ signal.

Once $M_{T2}^{\ell\ell}$ has been calculated, one can construct the invariant mass of the $2\ell + \cancel{E}_T$

system by using the MAOS momentum of the invisible particle given as

$$(m_h^{\text{maos}})^2 \equiv \left(p^\ell + q^\ell + k^{\text{maos}} + l^{\text{maos}} \right)^2, \quad (4.11)$$

which equals to m_h when $k^{\text{maos}} = k^{\text{true}}$ and $l^{\text{maos}} = l^{\text{true}}$. It is shown in the left panel in the lower frame of Figure 8. One can further employ the transverse mass of the leptonic system while ignoring the unknown $m_{\nu\nu}$ value and the longitudinal momentum components of neutrinos,

$$\left(M_T^{\ell\ell} \right)^2 = m_{\ell\ell}^2 + 2 \left(\sqrt{|\mathbf{p}_T^{\ell\ell}|^2 + m_{\ell\ell}^2} |\mathbf{p}_T| - \mathbf{p}_T^{\ell\ell} \cdot \mathbf{p}_T \right), \quad (4.12)$$

which is bounded from above by m_h [90]. Since both distributions have distinguishable peak and edge structures as well as a strong correlation with m_h , we use them as cut variables demanding $m_h^{\text{maos}} < 145$ GeV and 30 GeV $< M_T^{\ell\ell} < 125$ GeV for $m_H = 400$ GeV, and 60 GeV $< m_h^{\text{maos}} < 136$ GeV and 58 GeV $< M_T^{\ell\ell} < 126$ GeV for $m_H = 260$ GeV signal events. We have not applied the lower cut on m_h^{maos} for $m_H = 400$ GeV since the distribution is relatively distorted due to the trivial zero solutions described above.

After counting two b -jets as well as the charged leptons among the set of visible particle system, *i.e.*, $V = b\ell$, one can define another kind of the M_{T2} variable, denoted as $M_{T2}^{bb\ell\ell}$.¹⁰ Recall that M_{T2} aims at the physics processes describable by the decay topology (4.3). The Higgs signal has a different decay topology since the invisible particle system is disjointed from the $b\bar{b}$ system. On the other hand, it is well known that the di-leptonic $t\bar{t}$ process is the one of the SM processes where the M_{T2} variable is applicable since the decay topology is exactly the same as (4.3), and the $M_{T2}^{bb\ell\ell}$ distribution is strictly bounded from above by m_t . Therefore, one can still attempt to employ $M_{T2}^{bb\ell\ell}$ to reduce the $t\bar{t}$ backgrounds if the edge structure of the signal distribution has a certain amount of deviation from m_t . The $M_{T2}^{bb\ell\ell}$ distributions for both signal and $t\bar{t}$ are shown in the right panel of Figure 8.

Before going further, we here briefly summarize the types of the M_{T2} solutions for the invisible momenta. The hypothetical invisible momentum configuration that gives the M_{T2} value can be classified in two types. One is a balanced configuration, in which $M_T^{(1)} = M_T^{(2)}$ is realized, and the other is an unbalanced one, in which $M_T^{(1)} \neq M_T^{(2)}$ [77]. In each collider event, only one type of the momentum configuration provides the M_{T2} value, and it can be deduced by the invariant masses of the visible particle set in the event, m_V and $m_{\bar{V}}$ in eqs. (4.5). One can easily find that a stationary value of the transverse mass $M_T^{(1)}$ is attained when $\mathbf{k}_T = m_\chi \mathbf{p}_T / m_V$ and $\mathbf{l}_T = \mathbf{p}_T - \mathbf{k}_T$. Then,

$$M_T^{(1)} = m_V + m_\chi, \quad (4.13)$$

which is called an unconstrained minimum of the transverse mass. Similarly, one can find the stationary value of $M_T^{(2)} = m_{\bar{V}} + m_\chi$. For each stationary point, the $M_T^{(1)}$ value can

¹⁰ There is an ambiguity of how to pair one b -jet to one charged lepton because there can be two possible pairings in each event. Here, we define $M_{T2}^{bb\ell\ell}$ as the smaller one between two possible values of $M_{T2}^{bb\ell\ell}$. This definition matches the one used to measure the top quark mass using M_{T2} in [78].

be compared to $M_T^{(2)}$. In the case that

$$M_T^{(1)} \Big|_{\mathbf{k}_T = m_\chi \mathbf{p}_T / m_V} = m_V + m_\chi > M_T^{(2)} \Big|_{\mathbf{l}_T = \mathbf{p}_T - \mathbf{k}_T}, \quad (4.14)$$

M_{T2} is given by the unconstrained minimum of $M_T^{(1)}$, *i.e.*,

$$M_{T2} = m_V + m_\chi. \quad (4.15)$$

This corresponds to the unbalanced configuration. On the other hand, if it is satisfied that

$$\begin{aligned} M_T^{(1)} \Big|_{\mathbf{k}_T = m_\chi \mathbf{p}_T / m_V} &= m_V + m_\chi \leq M_T^{(2)} \Big|_{\mathbf{l}_T = \mathbf{p}_T - \mathbf{k}_T}, \\ M_T^{(2)} \Big|_{\mathbf{l}_T = m_\chi \mathbf{q}_T / m_{\bar{V}}} &= m_{\bar{V}} + m_\chi \leq M_T^{(1)} \Big|_{\mathbf{k}_T = \mathbf{p}_T - \mathbf{l}_T}, \end{aligned} \quad (4.16)$$

then M_{T2} is given by the balanced configuration in which $M_T^{(1)} = M_T^{(2)}$. See refs. [77, 91–93] for the detailed discussion of the momentum configuration types and their corresponding properties of M_{T2} .

In the case of $M_{T2}^{\ell\ell}$, the M_{T2} value is always given by the balanced configuration since $m_\ell = m_\nu = 0$. On the other hand, because $m_{b\ell}$ is not a constant but a variable, there exist sort of events in which the unbalanced configuration is selected to provide the $M_{T2}^{bb\ell\ell}$ value. In the di-leptonic $t\bar{t}$ process,

$$m_{b\ell} \leq \sqrt{m_t^2 - m_W^2} \simeq 154 \text{ GeV} \quad (4.17)$$

when the b quark mass is neglected. Therefore, the unbalanced $M_{T2}^{bb\ell\ell}$ has a maximum value smaller than m_t , while the balanced M_{T2} value can be as large as m_t . This means that the overall $M_{T2}^{bb\ell\ell}$ distribution is bounded from above by the maximum of the balanced $M_{T2}^{bb\ell\ell}$ values. For the Higgs signal, the situation is different. If one considers the case when the total transverse momentum of whole system is vanishing, or identically, the heavy Higgs has been produced at rest on the transverse plane, one can find that the balanced $M_{T2}^{bb\ell\ell}$ value cannot exceed $m_H/2$ by a similar consideration as done in Appendix A. However, by eq. (4.15), the unbalanced $M_{T2}^{bb\ell\ell}$ has an upper bound at $m_{b\ell}^{\max}$, which can be expressed analytically as

$$m_{b\ell}^{\max} = \frac{m_H m_W}{2m_h} \left(1 + \sqrt{1 - \frac{4m_h^2}{m_H^2}} \right) \simeq 229 \text{ GeV} \quad (4.18)$$

for $m_H = 400 \text{ GeV}$, while it is $\simeq 107 \text{ GeV}$ for $m_H = 260 \text{ GeV}$. The maximum value in the above equation is achieved when one of the hypothetical neutrino momenta chosen by the $M_{T2}^{bb\ell\ell}$ calculation is parallel to the momentum direction of the charged lepton sharing the same parent particle, while the other one is anti-parallel.¹¹ The $m_{b\ell}$ distributions for various m_H values and the $M_{T2}^{bb\ell\ell}$ distributions classified by the types of the $M_{T2}^{bb\ell\ell}$ solutions are shown in Figure 9, using the parton-level data for the sake of a numerical

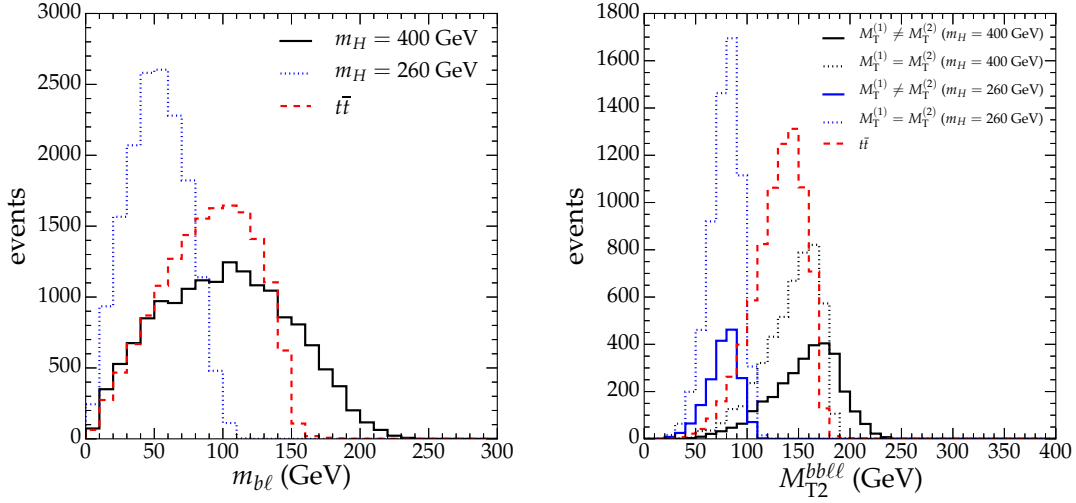


Figure 9. Parton-level distributions for (Left panel) $m_{b\ell}$ when $m_H = 260$ and 400 GeV and (Right panel) $M_{T2}^{bb\ell\ell}$ classified by the types of the invisible momentum configuration chosen by the M_{T2} calculation. See the text for detailed explanation. For a comparison, distributions for the di-leptonic $t\bar{t}$ process are shown.

demonstration. This also means that the endpoint of $M_{T2}^{bb\ell\ell}$ as well as the $m_{b\ell}$ distributions for the Higgs signal events will be smaller than m_t if $m_H \lesssim 330$ GeV, and in that case, the upper cut instead of the lower one should be used unless the upper bound value is too close to m_t . This observation may lead one to deduce that the efficiency of the $M_{T2}^{bb\ell\ell}$ cut might be the similar as that of the $m_{b\ell}$ cut. However, in our numerical study, the $M_{T2}^{bb\ell\ell}$ cut turns out to perform slightly better than $m_{b\ell}$. This might be because $M_{T2}^{bb\ell\ell}$ incorporates the effect of the missing momentum and its correlation with the visible momenta. We set the event selection cut value as $M_{T2}^{bb\ell\ell} > 165$ GeV for $m_H = 400$ GeV and $M_{T2}^{bb\ell\ell} < 96$ GeV for $m_H = 260$ GeV signals.

When considering final-state particles all together, the simplest kinematic variables that one can construct are the invariant mass of total visible system, $m_{bb\ell\ell}$, and the transverse mass of the full system including the missing energy. Since the full visible + invisible system has a fixed invariant mass, *i.e.*, m_H , the invariant mass of the visible system also has a dependency on m_H for its maximal value. One can find that

$$m_{bb\ell\ell}^2 \leq \frac{m_H^2}{2} \left(1 + \sqrt{1 - \frac{4m_h^2}{m_H^2}} \right) \simeq (377 \text{ GeV})^2 \quad (4.19)$$

for $m_H = 400$ GeV, whereas there is no definite cut-off in the $t\bar{t}$ background since $m_{t\bar{t}}$ is a variable of the event in the hadron collider. See the left panel of Figure 10. Since the lower bound is fixed as $m_{b\bar{b}} = m_h = 125$ GeV in the signal events, only upper cut on $m_{bb\ell\ell}$

¹¹We note that this $m_{b\ell}^{\max}$ for the Higgs signal is not a global maximum for all possible $b\ell$ pairings, but the maximum for a pair which leads to the smaller value of $M_{T2}^{bb\ell\ell}$.

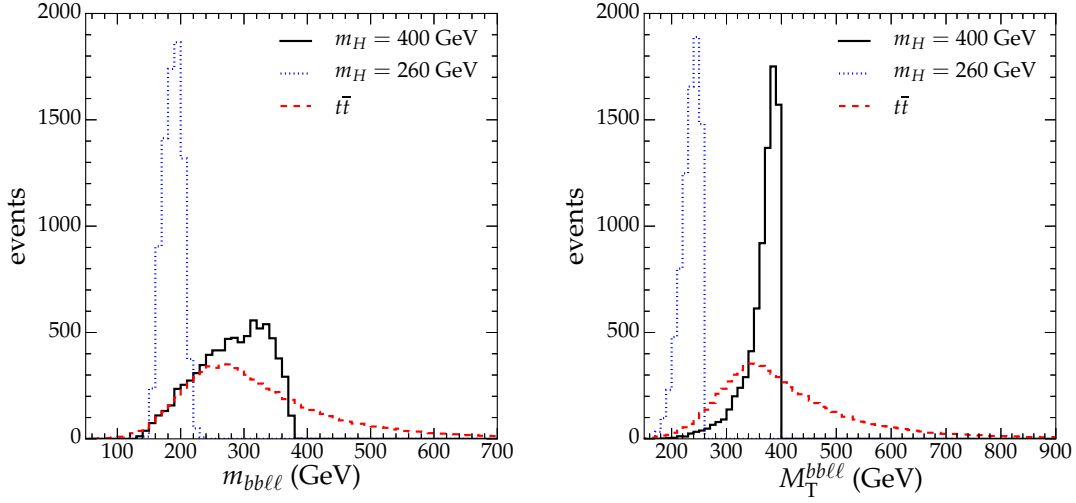


Figure 10. Normalized distributions for (Left panel) $m_{bb\ell\ell}$ and (Right panel) $M_T^{bb\ell\ell}$ distributions for $m_H = 260$ and 400 GeV and the $t\bar{t}$ backgrounds using parton-level data.

variable can be applied. For the benchmark point with $m_H = 400$ (260) GeV, we set the cut as $m_{bb\ell\ell} < 395$ (200) GeV. This cut becomes important in the case of a heavy Higgs with lower mass value like in the case of $m_H = 260$ GeV since it is capable of taking more stronger cut value. The other useful kinematic variable is the transverse mass of the full system defined as

$$\left(M_T^{bb\ell\ell}\right)^2 = m_{bb\ell\ell}^2 + 2 \left(\sqrt{|\mathbf{p}_T^{bb\ell\ell}|^2 + m_{bb\ell\ell}^2} |\mathbf{p}_T| - \mathbf{p}_T^{bb\ell\ell} \cdot \mathbf{p}_T \right), \quad (4.20)$$

where $\mathbf{p}_T^{bb\ell\ell} \equiv \mathbf{p}_T^b + \mathbf{p}_T^{\bar{b}} + \mathbf{p}_T^\ell + \mathbf{q}_T^\ell$ is the total visible transverse momentum. Here, the unknown $m_{\nu\nu}$ is ignored. When all the visible particles are on the transverse plane and the neutrino momentum vectors are collinear so that the $m_{\nu\nu}$ is vanishing, the transverse mass is equivalent to the invariant mass of the full system, *i.e.*, m_H . It means that the transverse mass is bounded from above by m_H as can be seen in the right panel of Figure 10. In real situation, the endpoint of the distribution is often smeared by the backgrounds and/or poor reconstruction efficiency of the final-state objects. Still, since the peak position is near the endpoint, it can provide an lower bound on m_H . On the other hand, the transverse mass has some correlation with the MAOS invariant mass as discussed in [83]. They select the similar types of events in the phase space, and the efficiency is comparable to each other. We employ both two variables to suppress backgrounds and define the signal region.

Combining all the cuts discussed so far, we examine their effects on the signal and the backgrounds by investigating how the cross sections are changing by applying event selection cuts. See Tables 3 and 4 for $m_H = 400$ and 260 GeV, respectively. The unlisted backgrounds turned out to be almost negligible after applying the initial cuts. In summary, although the production cross section for $m_H = 400$ GeV is smaller than that of $m_H = 260$

Selection cuts	$H \rightarrow hh$	$t\bar{t}$	GGF h	$h t\bar{t}$	hh	DY	VV	$\hat{\sigma}_{3000}$
Basic selection	0.54	3560.36	0.15	0.072	0.024	272.41	0.90	0.48
$\Delta\phi_{\ell\ell}, \Delta R_{\ell\ell}, p_{\text{T}}^{\ell\ell}$	0.40	562.02	0.11	0.015	0.019	33.56	0.047	0.90
$m_{\ell\ell}, M_{\text{T}2}^{\ell\ell}$	0.36	314.95	0.097	0.009	0.017	11.20	0.0	1.1
$m_h^{\text{maos}}, M_{\text{T}}^{\ell\ell}$	0.33	237.96	0.097	0.007	0.015	11.20	–	1.2
$\Delta R_{bb}, p_{\text{T}}^{bb}$	0.23	73.03	0.008	0.002	0.012	3.73	–	1.4
m_{bb}	0.14	16.24	0.0	$\simeq 0.0$	0.007	0.0	–	1.9
$\Delta\phi_{bb,\ell\ell}, m_{bb\ell\ell}$	0.13	11.99	–	–	0.005	–	–	2.1
$M_{\text{T}2}^{bb\ell\ell}$	0.059	1.31	–	–	0.004	–	–	2.8
Signal region	0.048	0.70	–	–	$\simeq 0.0$	–	–	3.1

Table 3. Cut flow of signals for $m_H = 400$ GeV and the main backgrounds in fb. See the text for detailed description of the event selection cuts applied. VV denotes the di-boson processes ($V = W, Z$). $\hat{\sigma}_{3000}$ is the signal significance calculated with a Poisson probability at 3000 fb^{-1} integrated luminosity. The signal region is defined by $345 \text{ GeV} < M_{\text{T}}^{bb\ell\ell} < 425 \text{ GeV}$ and $350 \text{ GeV} < m_H^{\text{maos}} < 430 \text{ GeV}$.

GeV, the signal can be distinguished by several angular cut variables as well as the cut on $M_{\text{T}2}^{bb\ell\ell}$. We have found a set of kinematic variables useful for the search. Eventually, the scenarios with a relatively lighter singlet-like Higgs boson are quite difficult to probe by using the kinematic event variables. In this case, one can still attempt to combine the search results from the other channels like $bb\tau\tau$ and $bbZZ$, which have the next-to-subleading branching fractions, or a multivariate analysis like performed in [88]. If m_H is much larger than 400 GeV, it is expected that the boosted Higgs technique approach is more promising.

Up to now, we have assumed that $\text{BR}(H \rightarrow hh) \sim 1$. This can be fulfilled in a large $(\lambda_{22}, \lambda_{03}, \lambda_{03})$ parameter-space region. We now relax this condition and suppose that the SM Higgs-like decays originated by the mixing are non-negligible. In this case, for a given m_H value, we can evaluate bounds on the mixing using the ATLAS and CMS data on heavy Higgs searches [16], as shown in Figure 3. The most stringent exclusion limit comes from the CMS search [18, 19]. This search is focused on the combination of the $4\ell/2\ell 2\tau$ final states in the $H \rightarrow ZZ$ channel assuming that the heavy Higgs only decays into SM particles, *i.e.*, $\text{BR}(H \rightarrow hh)$ is vanishing. The maximal mixing angle allowed by this search for $m_H = 260$ GeV is $\sin^2 \alpha < 0.06$ (95% C.L.), while for $m_H = 400$ GeV it is $\sin^2 \alpha < 0.11$ (95% C.L.). If $\text{BR}(H \rightarrow hh)$ is non-vanishing, the latter constraints become weaker. The excluded $\sin^2 \alpha$ values for given $\text{BR}(H \rightarrow hh)$ are represented in the light gray

Selection cuts	$H \rightarrow hh$	$t\bar{t}$	GGF h	$h t\bar{t}$	hh	DY	VV	$\hat{\sigma}_{3000}$
Basic selection	0.48	3560.36	0.15	0.072	0.024	272.41	0.90	0.43
$\Delta\phi_{\ell\ell}, \Delta R_{\ell\ell}, p_{\text{T}}^{\ell\ell}$	0.28	818.01	0.15	0.020	0.022	48.51	0.095	0.70
$m_{\ell\ell}, M_{\text{T}2}^{\ell\ell}$	0.21	206.23	0.11	0.006	0.007	0.0	0.0	0.80
$m_h^{\text{maos}}, M_{\text{T}}^{\ell\ell}$	0.19	140.69	0.08	0.004	0.005	–	–	0.88
$\Delta R_{bb}, m_{bb}$	0.104	6.65	0.008	$\simeq 0.0$	$\simeq 0.0$	–	–	2.21
$m_{bb\ell\ell}$	0.009	3.03	0.008	–	–	–	–	2.82
$M_{\text{T}2}^{bb\ell\ell}$	0.083	2.29	0.0	–	–	–	–	2.99
Signal region	0.083	2.19	–	–	–	–	–	3.06

Table 4. Cut flow of signals for $m_H = 260$ GeV and the main backgrounds in fb. See the text for detailed description of the event selection cuts applied. $\hat{\sigma}_{3000}$ is the signal significance calculated with a Poisson probability at 3000 fb^{-1} integrated luminosity. The signal region is defined by $180 \text{ GeV} < M_{\text{T}}^{bb\ell\ell} < 265 \text{ GeV}$ and $185 \text{ GeV} < m_H^{\text{maos}} < 305 \text{ GeV}$.

region in Figure 11 for both $m_H = 260$ GeV and $m_H = 400$ GeV. On the other hand, the constraints imposed by the EWPO and the LHC, shown as dark gray region in Figure 11, are independent of $\text{BR}(H \rightarrow hh)$. This is because they come from the modification of the couplings, parameterized by the mixing angle α , while the ones derived from the heavy Higgs searches depend directly on the value of $\text{BR}(H \rightarrow hh)$. One can also see the interplay between direct and indirect constraints in Figure 11. For $m_H = 260$ GeV, the direct search result on $H \rightarrow ZZ$ imposes the most stringent bound, up to $\text{BR}(H \rightarrow hh) \sim 0.4$. For larger values of $\text{BR}(H \rightarrow hh)$, the LHC + EWPO limits are the most important since the direct search limit weakens. For $m_H = 400$ GeV the direct limit is not as stringent as the indirect ones, which impose an upper bound of $\sin^2 \alpha < 0.084$, independently of the $\text{BR}(H \rightarrow hh)$ value.

We can use the discovery reach of the 14 TeV LHC [94] for the Higgs boson search using the decay channel $H \rightarrow ZZ \rightarrow 4\ell$ in order to estimate the detectability of the two m_H values as a function of the mixing and the $\text{BR}(H \rightarrow hh)$.¹² In Figure 11, we show the 3σ and 5σ significance lines for this channel for the integrated luminosity of 3000 fb^{-1} . These lines show that for low values of $\text{BR}(H \rightarrow hh)$ this search is able to resolve a large portion of the mixing angle values, leaving a small window of possible values. The sensitivity of this channel begin to decrease for $\text{BR}(H \rightarrow hh) > 0.6$, just in the region where the double Higgs production, in particular the channel above mentioned, becomes relevant. In Figure 11, we have included the 3σ equivalent line for the $H \rightarrow hh \rightarrow b\bar{b}WW^*$ channel. It is important

¹²We assume that $\text{BR}(H \rightarrow hh) + \text{BR}(H \rightarrow \text{SM particles}) = 1$.

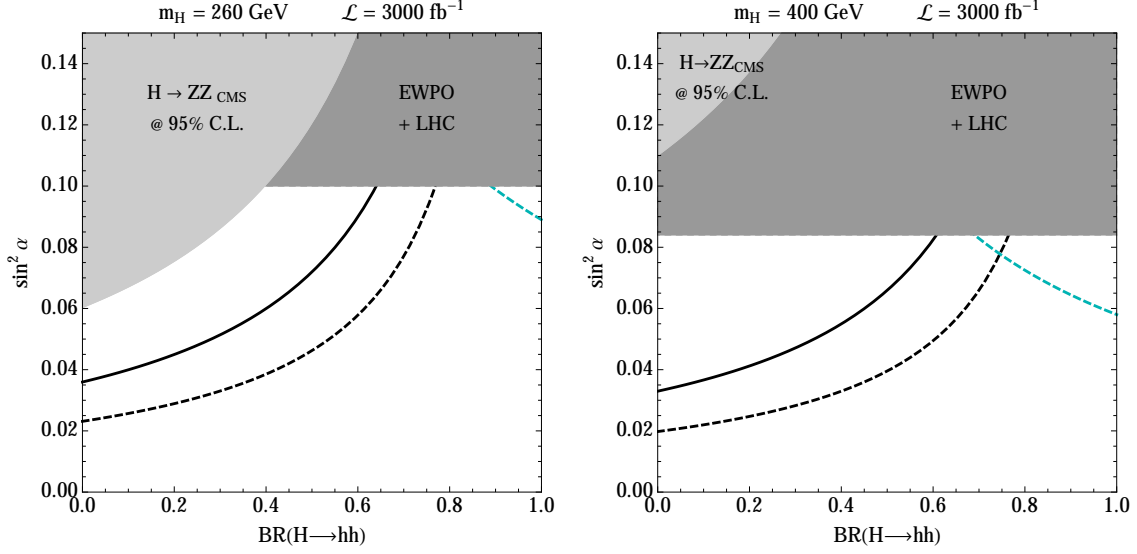


Figure 11. The dashed line delimits the 3σ significance region in the $\sin^2 \alpha - \text{BR}(H \rightarrow hh)$ plane for the $H \rightarrow hh \rightarrow b\bar{b}WW^* \rightarrow 2b + 2\ell + 2\nu$ ($\ell = e, \mu$) process for the integrated luminosity of 3000 fb^{-1} . The solid (dashed) black curve corresponds to the 5σ (3σ) for the $H \rightarrow ZZ \rightarrow 4\ell/2\ell 2\tau$ channels. Dark grey shaded region is the 95% C.L. CMS exclusion bounds and the light grey region is the one for EWPO + LHC.

to note that both channels are complementary since they are very dependent on the value of $\text{BR}(H \rightarrow hh)$. As a remark the ATLAS collaboration has performed a search of heavy Higgses using the channel $H \rightarrow hh \rightarrow b\bar{b}\gamma\gamma$ [95]. The results are not shown because the exclusion limit is well above the ones appeared in Figure 11.

5 Comments on Dark Matter

Given that the new scalar is unstable, it does not solve the dark matter problem. Nevertheless, it can play a relevant role by providing a portal to DM. In this section we explore this possibility. The DM mass and its coupling to the new scalar will be restricted by requiring a DM relic density in agreement with the experimental value. We analyse the compatibility between this condition and the requirement of a sizable $H \rightarrow hh$ branching ratio, as assumed in the previous section.

Let us consider an extra singlet neutral Dirac fermion transforming under a Z_2 symmetry. There is a unique even renormalizable interaction term, so the Lagrangian gets enlarged by

$$\bar{\psi}(i\not{\partial} - m_0)\psi + \lambda_\psi S\bar{\psi}\psi. \quad (5.1)$$

The singlet fermion is stable due to the Z_2 parity and is then a potential, WIMP-like, DM candidate.

5.1 Relic density

We have implemented the model in CALCHEP [96] and used the MICROMEGAS 2.4 package [97] to evaluate the DM relic density for the two benchmark points studied in the previous section. The results are displayed in Figure 12, where we show the DM relic density as a function of the WIMP mass, m_ψ , for different values of λ_ψ . The light red region corresponds to λ_ψ values varying from 0.001 to 1. The black solid line represents the relic density for $\lambda_\psi = 0.1$. The blue band is bounded by the allowed experimental relic density value given by Planck [98]:

$$0.1134 < \Omega h^2 < 0.1258 \quad (95\% \text{ C.L.}) \quad (5.2)$$

Note that the correct relic density can be achieved in two regions. The first one is characterized by a DM mass close to $m_h/2$, providing an enhancement of the DM annihilation cross section due to the resonance effect. When kinematically allowed, the Higgs decay into a ψ pair becomes to be dominant. As the LHC constrains the Higgs invisible width, that is mainly given by

$$\Gamma(h \rightarrow \psi\bar{\psi}) = \frac{|\lambda_\psi \sin \alpha|^2}{16\pi} m_h \left(1 - \frac{4m_\psi^2}{m_h^2}\right)^{3/2}, \quad (5.3)$$

this small m_ψ window gets reduced (~ 1 GeV).

There is a much wider parameter region where the enough amount of DM annihilation can be triggered by the heavy Higgs. Around and above the region of the heavy Higgs resonance, *i.e.*, $2m_\psi \gtrsim m_H$, the other annihilation channels such as $\psi\bar{\psi} \rightarrow hH$ and $\psi\bar{\psi} \rightarrow HH$ are open, thus making the DM annihilation sufficient to attain the correct relic density. For $2m_\psi < m_H$, the $H \rightarrow \psi\psi$ decay process will contribute to the decay width of the heavy Higgs boson, reducing the $\text{BR}(H \rightarrow hh)$ ratio and then decreasing the resonant double Higgs production. This could affect the analysis done in the previous sector by reducing the statistical significance of the signal. However in the region where $2m_\psi > m_H$ the results would remain unaffected. For this reason we should incorporate the constraints from the direct detection experiments in order to know which DM regions are favoured. A similar study was done in [99], that agrees with our analysis.

5.2 Direct Detection

Direct detection experiments search for DM by means of its elastic scattering off nuclei. In the absence of a positive signal, present search results translate into bounds on the WIMP-nuclei cross section for a given WIMP mass. As the elastic scattering is produced at low momentum we can write the interaction as an effective operator. In our case, it is induced by t -channel exchange of the Higgses and is given by:

$$\mathcal{L}_{\text{eff}} \supset \alpha_{q_i} \bar{\psi}\psi \bar{q}_i q_i, \quad (5.4)$$

with [12]

$$\frac{\alpha_q}{m_q} = \frac{\lambda_\psi \cos \alpha \sin \alpha}{v} \left(\frac{1}{m_h^2} - \frac{1}{m_H^2} \right), \quad (5.5)$$

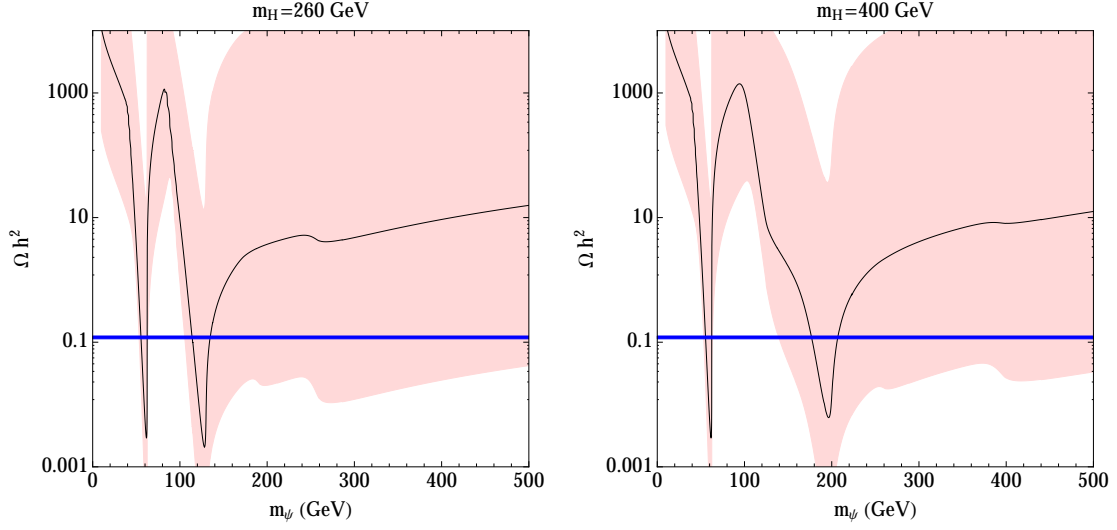


Figure 12. DM relic density as a function of the WIMP mass, m_ψ , for different values of λ_ψ . See the text for detailed description.

The spin-independent elastic scattering cross section can be written as¹³

$$\sigma_{\psi p}^{\text{SI}} = \frac{1}{\pi} \frac{m_p^2}{(m_p + m_\psi)^2} f_p^2, \quad (5.6)$$

where m_p is the proton mass and f_p is defined as

$$\frac{f_p}{m_p} = \sum_{q_i=u,d,s} f_{Tq_i}^p \frac{\alpha_{q_i}}{m_{q_i}} + \frac{2}{27} f_{TG}^p \sum_{q_i=c,b,t} \frac{\alpha_{q_i}}{m_{q_i}} \quad (5.7)$$

where the quantities f_{Tq_i} represent the contributions of the light quarks to the mass of the proton. The full expressions for the spin-independent cross section can be found in refs. [12, 14]. In Figure 13 the normalized spin-independent cross section is plotted as a function of the DM candidate mass for the two benchmark points. This normalized cross section, $\xi \sigma_{\psi N}^{\text{SI}}$, is the product of the spin-independent cross section and the factor ξ defined as $\xi \equiv \min\{1, \Omega_\psi h^2 / 0.1226\}$. This factor accounts for situations where ψ provides only a fraction of the total amount of dark matter. In Figure 13 a scan over the mass and the λ_ψ parameters has been done. Only the points with a relic density equal or less than that from Planck are showed. The bounds imposed by LUX [101] are included as well as future prospect from XENON 1T [102].

For the light DM candidate it is difficult to have the correct relic density and avoid the bound imposed by LUX at the same time. These conditions are compatible in a small region close to half of the mass of the Higgses so a resonant peak is present. However, this means that the decays $h \rightarrow \psi\bar{\psi}$ and $H \rightarrow \psi\bar{\psi}$ are dominant, so the model could be excluded

¹³See, for example, ref. [100]

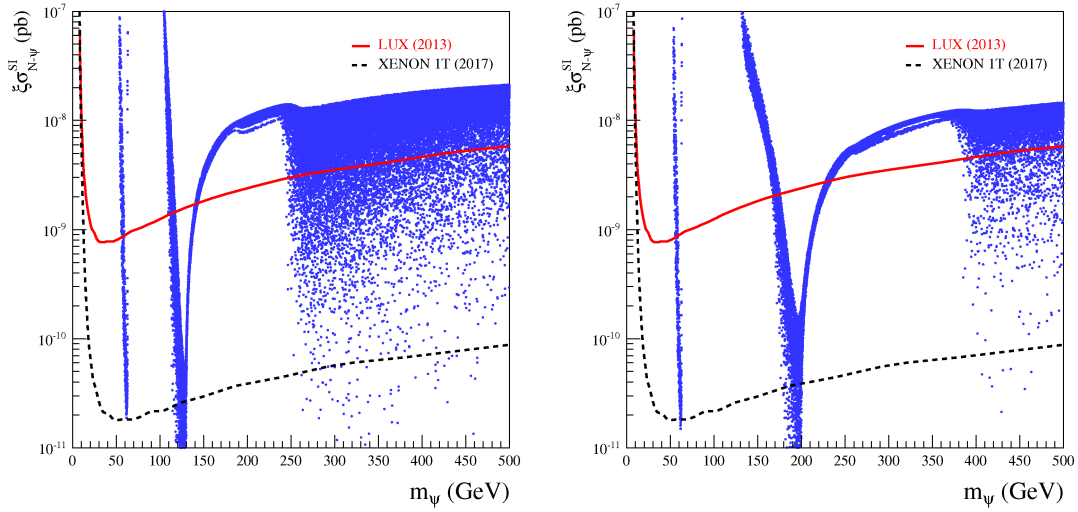


Figure 13. Spin independent cross section as function of the DM mass for the two different scenarios with $m_H = 260$ GeV (left) and $m_H = 400$ GeV (right). The red line represents the bounds from LUX [101] while the black dashed line corresponds to the future prospects of XENON1T [102].

by the LHC or would spoil the results obtained in the collider analysis. Nevertheless we can find a region with relatively high masses of the DM candidate that fulfills both relic density and spin-independent cross section and is placed above the resonance produced by the heavy Higgs. In fact, the allowed area is induced by the opening of the $\psi\bar{\psi} \rightarrow HH$ annihilation channel, making the cross section more effective.

To summarize, our analysis implies that there is a region where DM requirements are fulfilled and is located above the heavy Higgs mass so the constraints from the LHC and the results obtained in the collider analysis are not affected. Furthermore we can see that in the next years direct detection experiments such as XENON1T are sensitive to a large amount of the parameter space of this model, leading to the possibility of probing it.

6 Conclusions

In the coming years, the LHC will further explore the properties of the Higgs boson by looking for possible deviation from the SM predictions [103]. In particular, after the high-luminosity upgrade LHC is expected to deliver 3000 fb^{-1} at 14 TeV [104]. This would allow to measure the $\gamma\gamma$, WW , ZZ , $b\bar{b}$, and $\tau^+\tau^-$ Higgs couplings within a 2 – 8% error [103, 104]. Meanwhile, the singlet-extended model is the simplest extension of the SM scalar sector. It predicts a universal deficit in the Higgs boson couplings to the SM fermions and gauge bosons caused by the mixing between the two neutral scalar states. Alternatively, a new contribution to the invisible Higgs width would imply the reduction of the visible Higgs decays, that can also be interpreted as a generic Higgs coupling deficit. The direct production and detection of the new Higgs would certainly elucidate this point. Since

the relevant cross section depends on the mass and the mixing, we have first reviewed the present experimental bounds on these two parameters. Concerning the constraints by EWPO, we have improved previous analysis by using the full set of electroweak observables instead of the oblique parameters (S, T) since the last ones only provide an accurate descriptions of the heavy Higgs effects in the $m_H \sim m_h$ region.

In order to illustrate the detection of the direct heavy Higgs production, we have chosen two benchmark points compatible with present bounds, in particular, the LHC Higgs data and the EWPO. We have studied the resonant SM Higgs boson pair production in the $hh \rightarrow b\bar{b} WW \rightarrow b\bar{b}\ell^+\nu\ell^-\bar{\nu}$ decay channel. The main background to the signal is the di-leptonic $t\bar{t}$ process. Besides some basic selection cuts, we have applied M_{T2} cuts for the $2\ell + \cancel{E}_T$ or $2b + 2\ell + \cancel{E}_T$ systems to optimise the signal significance. Using the di-leptonic channel alone, a significance $\sim 3\sigma$ for 3000 fb^{-1} can be achieved at the 14 TeV LHC for $m_H = 400 \text{ GeV}$ if the mixing is close to its present limit and $\text{BR}(H \rightarrow hh) \approx 1$. A lower branching ratio or a smaller mixing angle would require combining various hh decay channels. The complementarity between $H \rightarrow hh$ and $H \rightarrow ZZ$ channels is studied for arbitrary $\text{BR}(H \rightarrow hh)$ values.

We have also checked that it is possible to extend the model by including a DM candidate. The next generation of direct detection experiments will be capable of probing a large amount of the parameter space of the model.

Note added: After completion of this work, some similar results have been presented in [105].

Acknowledgments

VML is very grateful to the ZFITTER authors, specially to Tord Riemann, for useful and valuable explanations about ZFITTER program. JMM and VML are partially supported by the grants FPA2010-17747, FPA2012-34694, FPA2013-44773-P and from the Spanish MINECO, Consolider-Ingenio CPAN CSD2007-00042 and MULTIDARK CSD2009-00064 as well as the Centro de Excelencia Severo Ochoa Program under Grant No. SEV-2012-0249. VML also thanks support by the ERC Advanced Grant SPLE under contract ERC-2012-ADG-20120216-320421. The work of CBP was partially supported by the CERN-Korea fellowship through National Research Foundation of Korea.

Appendix

A Higgs M_{T2} in di-leptonic WW process

We here consider the maximum of M_{T2} in the di-leptonic decay mode of the $h \rightarrow WW^{(*)}$ process,

$$pp \rightarrow h + j \rightarrow WW^{(*)} + j \rightarrow \ell(p)\nu(k) + \ell(q)\nu(l) + j(u), \quad (\text{A.1})$$

where j denotes the initial state radiation, typically jets in the final state. The transverse components of the total momentum should be conserved and therefore

$$\mathbf{p}_T + \mathbf{k}_T + \mathbf{q}_T + \mathbf{l}_T + \mathbf{u}_T = \mathbf{0}. \quad (\text{A.2})$$

Since the visible particle in each decay chain, *i.e.*, the charged leptons are massless, the M_{T2} value is always achieved in a balanced configuration in which $M_T^{(1)} = M_T^{(2)}$ or

$$\begin{aligned} (|\mathbf{p}_T| + |\mathbf{k}_T^{\text{maos}}|)^2 - |\mathbf{p}_T + \mathbf{k}_T^{\text{maos}}|^2 &= (|\mathbf{q}_T| + |\mathbf{l}_T^{\text{maos}}|)^2 - |\mathbf{q}_T + \mathbf{l}_T^{\text{maos}}|^2, \\ \mathbf{k}_T^{\text{maos}} + \mathbf{l}_T^{\text{maos}} &= -\mathbf{p}_T - \mathbf{q}_T - \mathbf{u}_T, \end{aligned} \quad (\text{A.3})$$

where $\mathbf{k}_T^{\text{maos}}$ and $\mathbf{l}_T^{\text{maos}}$ stand for the M_{T2} solution for the invisible transverse momenta. The above equations are satisfied when $\mathbf{k}_T^{\text{maos}} = -\mathbf{q}_T$ and $\mathbf{l}_T^{\text{maos}} = -\mathbf{p}_T$ for vanishing \mathbf{u}_T . On the other hand, if \mathbf{u}_T is sizable, the solution can be redefined as

$$\begin{aligned} \mathbf{k}_T^{\text{maos}} &= -\mathbf{q}_T - \frac{\mathbf{u}_T}{2} - \delta\mathbf{u}_T \\ \mathbf{l}_T^{\text{maos}} &= -\mathbf{p}_T - \frac{\mathbf{u}_T}{2} + \delta\mathbf{u}_T. \end{aligned} \quad (\text{A.4})$$

where $\delta\mathbf{u}_T$ is a function parameterizing the transverse boost effect of the solution by \mathbf{u}_T while preserving conditions (A.3) and $\delta\mathbf{u}_T(\mathbf{u}_T = \mathbf{0}) = 0$.¹⁴ This solution is generically different from the true invisible momenta, *i.e.*, $\mathbf{k}_T^{\text{maos}} \neq \mathbf{k}_T$ and $\mathbf{l}_T^{\text{maos}} \neq \mathbf{l}_T$, however by construction, the sum of each component must be equal,

$$\mathbf{k}_T^{\text{maos}} + \mathbf{l}_T^{\text{maos}} = \mathbf{k}_T + \mathbf{l}_T. \quad (\text{A.5})$$

The maximum value of M_{T2} for given visible momenta and the sum of invisible momenta can be deduced from a kinematic property as given below,

$$M_T \leq m_h, \quad (\text{A.6})$$

where M_T and m_h are the transverse and the invariant masses for two charged leptons and two neutrinos defined as

$$\begin{aligned} M_T^2 &= \left(M_T^{(1)}\right)^2 + \left(M_T^{(2)}\right)^2 + 2\sqrt{|\mathbf{p}_T + \mathbf{k}_T^{\text{maos}}|^2 + \left(M_T^{(1)}\right)^2} \sqrt{|\mathbf{q}_T + \mathbf{l}_T^{\text{maos}}|^2 + \left(M_T^{(2)}\right)^2} \\ &\quad - 2(\mathbf{p}_T + \mathbf{k}_T^{\text{maos}}) \cdot (\mathbf{q}_T + \mathbf{l}_T^{\text{maos}}), \\ m_h^2 &= (p + k + q + l)^2, \end{aligned} \quad (\text{A.7})$$

respectively. The transverse mass can be further simplified as

$$M_T^2 = A^2 - |\mathbf{C}|^2 + B^2 - |\mathbf{D}|^2 + 2AB - 2\mathbf{C} \cdot \mathbf{D}, \quad (\text{A.8})$$

where

$$\begin{aligned} A &\equiv |\mathbf{p}_T| + |\mathbf{k}_T^{\text{maos}}|, \quad B \equiv |\mathbf{q}_T| + |\mathbf{l}_T^{\text{maos}}|, \\ \mathbf{C} &\equiv \mathbf{p}_T + \mathbf{k}_T^{\text{maos}}, \quad \mathbf{D} \equiv \mathbf{q}_T + \mathbf{l}_T^{\text{maos}}. \end{aligned} \quad (\text{A.9})$$

¹⁴ See [89] for the dedicated discussion of the M_{T2} solution in the case of fully massless visible and invisible particles.

One can see that the equations in (A.3) is satisfied for the kinematic configuration where

$$B = A, \quad \mathbf{D} = \epsilon \mathbf{C} \quad (\epsilon^2 = 1). \quad (\text{A.10})$$

Here, $\epsilon = -1$ corresponds to a kinematic configuration with vanishing \mathbf{u}_T , while it is non-vanishing and $\delta \mathbf{u}_T = \mathbf{p}_T - \mathbf{q}_T$ in the case of $\epsilon = 1$. Then, it is true that

$$M_T^2 = 4A^2 - 4|\mathbf{C}|^2 - (\epsilon - 1)(\epsilon + 3)|\mathbf{C}|^2 \geq 4A^2 - 4|\mathbf{C}|^2 = 4 \left(M_T^{(1)} \right)^2. \quad (\text{A.11})$$

for both cases. Since $M_{T2} = M_T^{(1)} = M_T^{(2)}$, the relation (A.6) implies that

$$M_{T2} \leq \frac{m_h}{2}, \quad (\text{A.12})$$

where the equality holds when eqs. (A.10) are satisfied. Up to now, we have not made any assumption whether the parent W boson is on-shell. In the case that both W bosons are on-shell, M_{T2} is bounded from above by m_W . Collectively, one can express the maximum of M_{T2} as

$$M_{T2} \leq \min \left\{ m_W, \frac{m_h}{2} \right\}. \quad (\text{A.13})$$

References

- [1] **ATLAS Collaboration** Collaboration, G. Aad et al., *Observation of a new particle in the search for the Standard Model Higgs boson with the ATLAS detector at the LHC*, *Phys.Lett. B* **716** (2012) 1–29, [[arXiv:1207.7214](#)].
- [2] **CMS Collaboration** Collaboration, S. Chatrchyan et al., *Observation of a new boson at a mass of 125 GeV with the CMS experiment at the LHC*, *Phys.Lett. B* **716** (2012) 30–61, [[arXiv:1207.7235](#)].
- [3] **ATLAS Collaboration** Collaboration, G. Aad et al., *Measurement of the Higgs boson mass from the $H \rightarrow \gamma\gamma$ and $H \rightarrow ZZ^* \rightarrow 4\ell$ channels with the ATLAS detector using 25 fb⁻¹ of pp collision data*, *Phys.Rev. D* **90** (2014) 052004, [[arXiv:1406.3827](#)].
- [4] **CMS Collaboration** Collaboration, V. Khachatryan et al., *Precise determination of the mass of the Higgs boson and tests of compatibility of its couplings with the standard model predictions using proton collisions at 7 and 8 TeV*, [[arXiv:1412.8662](#)].
- [5] P. Bechtle, S. Heinemeyer, O. Stl, T. Stefaniak, and G. Weiglein, *Probing the Standard Model with Higgs signal rates from the Tevatron, the LHC and a future ILC*, *JHEP* **1411** (2014) 039, [[arXiv:1403.1582](#)].
- [6] J. Elias-Miro, J. R. Espinosa, G. F. Giudice, H. M. Lee, and A. Strumia, *Stabilization of the Electroweak Vacuum by a Scalar Threshold Effect*, *JHEP* **1206** (2012) 031, [[arXiv:1203.0237](#)].
- [7] J. R. Espinosa, T. Konstandin, and F. Riva, *Strong Electroweak Phase Transitions in the Standard Model with a Singlet*, *Nucl.Phys. B* **854** (2012) 592–630, [[arXiv:1107.5441](#)].
- [8] J. M. Cline and K. Kainulainen, *Electroweak baryogenesis and dark matter from a singlet Higgs*, *JCAP* **1301** (2013) 012, [[arXiv:1210.4196](#)].

- [9] P. H. Damgaard, D. O’Connell, T. C. Petersen, and A. Tranberg, *Constraints on New Physics from Baryogenesis and Large Hadron Collider Data*, *Phys.Rev.Lett.* **111** (2013) 221804, [[arXiv:1305.4362](#)].
- [10] J. McDonald, *Gauge singlet scalars as cold dark matter*, *Phys.Rev.* **D50** (1994) 3637–3649, [[hep-ph/0702143](#)].
- [11] S. Baek, P. Ko, W.-I. Park, and E. Senaha, *Vacuum structure and stability of a singlet fermion dark matter model with a singlet scalar messenger*, *JHEP* **1211** (2012) 116, [[arXiv:1209.4163](#)].
- [12] Y. G. Kim, K. Y. Lee, and S. Shin, *Singlet fermionic dark matter*, *JHEP* **0805** (2008) 100, [[arXiv:0803.2932](#)].
- [13] L. Lopez-Honorez, T. Schwetz, and J. Zupan, *Higgs portal, fermionic dark matter, and a Standard Model like Higgs at 125 GeV*, *Phys.Lett.* **B716** (2012) 179–185, [[arXiv:1203.2064](#)].
- [14] M. Fairbairn and R. Hogan, *Singlet Fermionic Dark Matter and the Electroweak Phase Transition*, *JHEP* **1309** (2013) 022, [[arXiv:1305.3452](#)].
- [15] **The ATLAS Collaboration**, *Search for a high-mass Higgs boson in the $H \rightarrow WW \rightarrow l\nu l\nu$ decay channel with the ATLAS detector using 21 fb^{-1} of proton-proton collision data*, . <http://cds.cern.ch/record/1562879>.
- [16] **CMS Collaboration**, S. Chatrchyan et al., *Search for a standard-model-like Higgs boson with a mass in the range 145 to 1000 GeV at the LHC*, *Eur.Phys.J.* **C73** (2013) 2469, [[arXiv:1304.0213](#)].
- [17] **ATLAS Collaboration**, *Measurements of the properties of the Higgs-like boson in the four lepton decay channel with the ATLAS detector using 25 fb^{-1} of proton-proton collision data*, . <http://cds.cern.ch/record/1523699>.
- [18] **CMS Collaboration**, C. Collaboration, *Search for a standard model like Higgs boson in the decay channel H to ZZ to $l+l-$ $q \bar{q}$ at CMS*, . <http://cds.cern.ch/record/1564157>.
- [19] **CMS Collaboration**, *Properties of the Higgs-like boson in the decay H to ZZ to $4l$ in pp collisions at $\sqrt{s} = 7$ and 8 TeV* , . <http://cds.cern.ch/record/1523767>.
- [20] **CMS Collaboration**, *Update on the search for the standard model Higgs boson in pp collisions at the LHC decaying to $W + W$ in the fully leptonic final state*, .
- [21] M. Bowen, Y. Cui, and J. D. Wells, *Narrow trans-TeV Higgs bosons and $H \rightarrow hh$ decays: Two LHC search paths for a hidden sector Higgs boson*, *JHEP* **0703** (2007) 036, [[hep-ph/0701035](#)].
- [22] M. J. Dolan, C. Englert, and M. Spannowsky, *New Physics in LHC Higgs boson pair production*, *Phys.Rev.* **D87** (2013), no. 5 055002, [[arXiv:1210.8166](#)].
- [23] J. M. No and M. Ramsey-Musolf, *Probing the Higgs Portal at the LHC Through Resonant di-Higgs Production*, [arXiv:1310.6035](#).
- [24] G. M. Pruna and T. Robens, *The Higgs Singlet extension parameter space in the light of the LHC discovery*, *Phys.Rev.* **D88** (2013) 115012, [[arXiv:1303.1150](#)].
- [25] C.-Y. Chen, S. Dawson, and I. Lewis, *Exploring Resonant di-Higgs production in the Higgs Singlet Model*, [arXiv:1410.5488](#).

- [26] A. Hill and J. van der Bij, *Strongly interacting singlet-doublet Higgs model*, *Phys.Rev.* **D36** (1987) 3463–3473.
- [27] M. Veltman and F. Yndurain, *Radiative corrections to $W W$ scattering*, *Nucl.Phys.* **B325** (1989) 1.
- [28] T. Binoth and J. van der Bij, *Influence of strongly coupled, hidden scalars on Higgs signals*, *Z.Phys.* **C75** (1997) 17–25, [[hep-ph/9608245](#)].
- [29] R. Schabinger and J. D. Wells, *A Minimal spontaneously broken hidden sector and its impact on Higgs boson physics at the large hadron collider*, *Phys.Rev.* **D72** (2005) 093007, [[hep-ph/0509209](#)].
- [30] B. Patt and F. Wilczek, *Higgs-field portal into hidden sectors*, [hep-ph/0605188](#).
- [31] G. Bhattacharyya, G. C. Branco, and S. Nandi, *Universal Doublet-Singlet Higgs Couplings and phenomenology at the CERN Large Hadron Collider*, *Phys.Rev.* **D77** (2008) 117701, [[arXiv:0712.2693](#)].
- [32] V. Barger, P. Langacker, M. McCaskey, M. J. Ramsey-Musolf, and G. Shaughnessy, *LHC Phenomenology of an Extended Standard Model with a Real Scalar Singlet*, *Phys.Rev.* **D77** (2008) 035005, [[arXiv:0706.4311](#)].
- [33] V. Barger, P. Langacker, M. McCaskey, M. Ramsey-Musolf, and G. Shaughnessy, *Complex Singlet Extension of the Standard Model*, *Phys.Rev.* **D79** (2009) 015018, [[arXiv:0811.0393](#)].
- [34] S. Dawson and W. Yan, *Hiding the Higgs Boson with Multiple Scalars*, *Phys.Rev.* **D79** (2009) 095002, [[arXiv:0904.2005](#)].
- [35] S. Bock, R. Lafaye, T. Plehn, M. Rauch, D. Zerwas, et al., *Measuring Hidden Higgs and Strongly-Interacting Higgs Scenarios*, *Phys.Lett.* **B694** (2010) 44–53, [[arXiv:1007.2645](#)].
- [36] S. Baek, P. Ko, and W.-I. Park, *Search for the Higgs portal to a singlet fermionic dark matter at the LHC*, *JHEP* **1202** (2012) 047, [[arXiv:1112.1847](#)].
- [37] P. J. Fox, D. Tucker-Smith, and N. Weiner, *Higgs friends and counterfeits at hadron colliders*, *JHEP* **1106** (2011) 127, [[arXiv:1104.5450](#)].
- [38] C. Englert, T. Plehn, D. Zerwas, and P. M. Zerwas, *Exploring the Higgs portal*, *Phys.Lett.* **B703** (2011) 298–305, [[arXiv:1106.3097](#)].
- [39] C. Englert, J. Jaeckel, E. Re, and M. Spannowsky, *Evasive Higgs Maneuvers at the LHC*, *Phys.Rev.* **D85** (2012) 035008, [[arXiv:1111.1719](#)].
- [40] B. Batell, S. Gori, and L.-T. Wang, *Exploring the Higgs Portal with 10/fb at the LHC*, *JHEP* **1206** (2012) 172, [[arXiv:1112.5180](#)].
- [41] C. Englert, T. Plehn, M. Rauch, D. Zerwas, and P. M. Zerwas, *LHC: Standard Higgs and Hidden Higgs*, *Phys.Lett.* **B707** (2012) 512–516, [[arXiv:1112.3007](#)].
- [42] R. S. Gupta and J. D. Wells, *Higgs boson search significance deformations due to mixed-in scalars*, *Phys.Lett.* **B710** (2012) 154–158, [[arXiv:1110.0824](#)].
- [43] D. Bertolini and M. McCullough, *The Social Higgs*, *JHEP* **1212** (2012) 118, [[arXiv:1207.4209](#)].
- [44] B. Batell, D. McKeen, and M. Pospelov, *Singlet Neighbors of the Higgs Boson*, *JHEP* **1210** (2012) 104, [[arXiv:1207.6252](#)].

- [45] D. Y. Bardin, M. S. Bilenky, G. Mitselmakher, G. Mitselmakher, T. Riemann, et al., *A Realistic Approach to the Standard Z Peak*, *Z.Phys.* **C44** (1989) 493.
- [46] D. Y. Bardin, M. S. Bilenky, A. Chizhov, A. Sazonov, A. Sazonov, et al., *Analytic approach to the complete set of QED corrections to fermion pair production in $e^+ e^-$ annihilation*, *Nucl.Phys.* **B351** (1991) 1–48, [[hep-ph/9801208](#)].
- [47] D. Y. Bardin, M. S. Bilenky, A. Sazonov, Y. Sedykh, Y. Sedykh, et al., *QED corrections with partial angular integration to fermion pair production in $e^+ e^-$ annihilation*, *Phys.Lett.* **B255** (1991) 290–296, [[hep-ph/9801209](#)].
- [48] D. Y. Bardin, M. S. Bilenky, A. Chizhov, O. Fedorenko, S. N. Ganguli, et al., *ZFITTER: An Analytical program for fermion pair production in $e^+ e^-$ annihilation*, [hep-ph/9412201](#).
- [49] D. Y. Bardin, P. Christova, M. Jack, L. Kalinovskaya, A. Olchevski, et al., *ZFITTER v.6.21: A Semianalytical program for fermion pair production in $e^+ e^-$ annihilation*, *Comput.Phys.Comm.* **133** (2001) 229–395, [[hep-ph/9908433](#)].
- [50] A. Arbuzov, *Light pair corrections to electron positron annihilation at LEP / SLC*, [hep-ph/9907500](#).
- [51] A. Arbuzov, M. Awramik, M. Czakon, A. Freitas, M. Grunewald, et al., *ZFITTER: A Semi-analytical program for fermion pair production in $e^+ e^-$ annihilation, from version 6.21 to version 6.42*, *Comput.Phys.Comm.* **174** (2006) 728–758, [[hep-ph/0507146](#)].
- [52] ZFITTER support group, ZFITTER 6.43, June, 2008. <http://zfitter.desy.de>.
- [53] **ALEPH Collaboration, DELPHI Collaboration, L3 Collaboration, OPAL Collaboration, SLD Collaboration, LEP Electroweak Working Group, SLD Electroweak Group, SLD Heavy Flavour Group** Collaboration, S. Schael et al., *Precision electroweak measurements on the Z resonance*, *Phys.Rept.* **427** (2006) 257–454, [[hep-ex/0509008](#)].
- [54] **ALEPH Collaboration, DELPHI Collaboration, L3 Collaboration, OPAL Collaboration, LEP Electroweak Working Group** Collaboration, S. Schael et al., *Electroweak Measurements in Electron-Positron Collisions at W-Boson-Pair Energies at LEP*, [arXiv:1302.3415](#).
- [55] **Gfitter Group** Collaboration, M. Baak et al., *The global electroweak fit at NNLO and prospects for the LHC and ILC*, *Eur.Phys.J.* **C74** (2014), no. 9 3046, [[arXiv:1407.3792](#)].
- [56] D. Lopez-Val and T. Robens, *Delta r and the W-boson mass in the Singlet Extension of the Standard Model*, *Phys.Rev.* **D90** (2014) 114018, [[arXiv:1406.1043](#)].
- [57] B. W. Lee, C. Quigg, and H. Thacker, *Weak Interactions at Very High-Energies: The Role of the Higgs Boson Mass*, *Phys.Rev.* **D16** (1977) 1519.
- [58] B. Cooper, N. Konstantinidis, L. Lambourne, and D. Wardrope, *Boosted $hh \rightarrow b\bar{b}b\bar{b}$: a new topology in searches for TeV-scale resonances at the LHC*, *Phys.Rev.* **D88** (2013) 114005, [[arXiv:1307.0407](#)].
- [59] D. E. Ferreira de Lima, A. Papaefstathiou, and M. Spannowsky, *Standard model Higgs boson pair production in the $(b\bar{b})(b\bar{b})$ final state*, *JHEP* **1408** (2014) 030, [[arXiv:1404.7139](#)].
- [60] T. A. collaboration, *A search for resonant Higgs-pair production in the $b\bar{b}b\bar{b}$ final state in pp collisions at $\sqrt{s} = 8$ TeV*, . <http://cds.cern.ch/record/1666518>.
- [61] **CMS Collaboration** Collaboration, C. Collaboration, *Search for di-Higgs resonances*

decaying to 4 bottom quarks, . <http://cds.cern.ch/record/1748425/files/>.

- [62] **ATLAS Collaboration** Collaboration, G. Aad et al., *Search For Higgs Boson Pair Production in the $\gamma\gamma b\bar{b}$ Final State using pp Collision Data at $\sqrt{s} = 8$ TeV from the ATLAS Detector*, [arXiv:1406.5053](#).
- [63] **CMS Collaboration** Collaboration, C. Collaboration, *Search for the resonant production of two Higgs bosons in the final state with two photons and two bottom quarks*, . <http://inspirehep.net/record/1292910/files/>.
- [64] V. Barger, L. L. Everett, C. Jackson, A. Peterson, and G. Shaughnessy, *New physics in resonant production of Higgs boson pairs*, *Phys.Rev.Lett.* **114** (2015) 011801, [[arXiv:1408.0003](#)].
- [65] V. Barger, L. L. Everett, C. B. Jackson, A. D. Peterson, and G. Shaughnessy, *Measuring the 2HDM Scalar Potential at LHC14*, *Phys.Rev.* **D90** (2014) 095006, [[arXiv:1408.2525](#)].
- [66] **LHC Higgs Cross Section Working Group** Collaboration, S. Dittmaier et al., *Handbook of LHC Higgs Cross Sections: 1. Inclusive Observables*, [arXiv:1101.0593](#).
- [67] T. Sjostrand, S. Mrenna, and P. Z. Skands, *PYTHIA 6.4 Physics and Manual*, *JHEP* **0605** (2006) 026, [[hep-ph/0603175](#)].
- [68] H.-L. Lai, M. Guzzi, J. Huston, Z. Li, P. M. Nadolsky, et al., *New parton distributions for collider physics*, *Phys.Rev.* **D82** (2010) 074024, [[arXiv:1007.2241](#)].
- [69] **DELPHES 3** Collaboration, J. de Favereau et al., *DELPHES 3, A modular framework for fast simulation of a generic collider experiment*, *JHEP* **1402** (2014) 057, [[arXiv:1307.6346](#)].
- [70] M. Cacciari, G. P. Salam, and G. Soyez, *FastJet User Manual*, *Eur.Phys.J.* **C72** (2012) 1896, [[arXiv:1111.6097](#)].
- [71] M. Cacciari, G. P. Salam, and G. Soyez, *The Anti- $k(t)$ jet clustering algorithm*, *JHEP* **0804** (2008) 063, [[arXiv:0802.1189](#)].
- [72] **ATLAS Collaboration** Collaboration, *Measurement of the Mistag Rate with 5 fb⁻¹ of Data Collected by the ATLAS Detector*, . <http://cds.cern.ch/record/1435194>.
- [73] M. El-Kacimi and R. Lafaye, *Simulation of neutral Higgs pairs production processes in PYTHIA using HPAIR matrix elements*, .
- [74] S. Dawson, S. Dittmaier, and M. Spira, *Neutral Higgs boson pair production at hadron colliders: QCD corrections*, *Phys.Rev.* **D58** (1998) 115012, [[hep-ph/9805244](#)].
- [75] M. Czakon and A. Mitov, *Top++: A Program for the Calculation of the Top-Pair Cross-Section at Hadron Colliders*, *Comput.Phys.Commun.* **185** (2014) 2930, [[arXiv:1112.5675](#)].
- [76] C. Lester and D. Summers, *Measuring masses of semiinvisibly decaying particles pair produced at hadron colliders*, *Phys.Lett.* **B463** (1999) 99–103, [[hep-ph/9906349](#)].
- [77] A. Barr, C. Lester, and P. Stephens, *$m(T2)$: The Truth behind the glamour*, *J.Phys.* **G29** (2003) 2343–2363, [[hep-ph/0304226](#)].
- [78] W. S. Cho, K. Choi, Y. G. Kim, and C. B. Park, *Measuring the top quark mass with $m(T2)$ at the LHC*, *Phys.Rev.* **D78** (2008) 034019, [[arXiv:0804.2185](#)].
- [79] **CDF Collaboration** Collaboration, T. Aaltonen et al., *Top Quark Mass Measurement*

- using m_{T2} in the Dilepton Channel at CDF, *Phys.Rev.* **D81** (2010) 031102, [[arXiv:0911.2956](#)].
- [80] **ATLAS Collaboration** Collaboration, *Top quark mass measurement in the e channel using the m_{T2} variable at ATLAS*, .
 - [81] **CMS Collaboration** Collaboration, S. Chatrchyan et al., *Measurement of masses in the $t\bar{t}$ system by kinematic endpoints in pp collisions at $\sqrt{s} = 7$ TeV*, *Eur.Phys.J.* **C73** (2013) 2494, [[arXiv:1304.5783](#)].
 - [82] K. Choi, S. Choi, J. S. Lee, and C. B. Park, *Reconstructing the Higgs boson in dileptonic W decays at hadron collider*, *Phys.Rev.* **D80** (2009) 073010, [[arXiv:0908.0079](#)].
 - [83] K. Choi, J. S. Lee, and C. B. Park, *Measuring the Higgs boson mass with transverse mass variables*, *Phys.Rev.* **D82** (2010) 113017, [[arXiv:1008.2690](#)].
 - [84] H.-C. Cheng and Z. Han, *Minimal Kinematic Constraints and M_{T2}* , *JHEP* **0812** (2008) 063, [[arXiv:0810.5178](#)].
 - [85] W. S. Cho, K. Choi, Y. G. Kim, and C. B. Park, *M_{T2} -assisted on-shell reconstruction of missing momenta and its application to spin measurement at the LHC*, *Phys.Rev.* **D79** (2009) 031701, [[arXiv:0810.4853](#)].
 - [86] C. B. Park, *Reconstructing the heavy resonance at hadron colliders*, *Phys.Rev.* **D84** (2011) 096001, [[arXiv:1106.6087](#)].
 - [87] J. M. Butterworth, A. R. Davison, M. Rubin, and G. P. Salam, *Jet substructure as a new Higgs search channel at the LHC*, *Phys.Rev.Lett.* **100** (2008) 242001, [[arXiv:0802.2470](#)].
 - [88] A. Papaefstathiou, L. L. Yang, and J. Zurita, *Higgs boson pair production at the LHC in the $b\bar{b}W^+W^-$ channel*, *Phys.Rev.* **D87** (2013) 011301, [[arXiv:1209.1489](#)].
 - [89] C. G. Lester, *The transverse mass, $MT2$, in special cases*, *JHEP* **1105** (2011) 076, [[arXiv:1103.5682](#)].
 - [90] A. J. Barr, B. Gripaios, and C. G. Lester, *Measuring the Higgs boson mass in dileptonic W -boson decays at hadron colliders*, *JHEP* **0907** (2009) 072, [[arXiv:0902.4864](#)].
 - [91] C. Lester and A. Barr, *MTGEN: Mass scale measurements in pair-production at colliders*, *JHEP* **0712** (2007) 102, [[arXiv:0708.1028](#)].
 - [92] W. S. Cho, K. Choi, Y. G. Kim, and C. B. Park, *Gluino Transverse Mass*, *Phys.Rev.Lett.* **100** (2008) 171801, [[arXiv:0709.0288](#)].
 - [93] W. S. Cho, K. Choi, Y. G. Kim, and C. B. Park, *Measuring superparticle masses at hadron collider using the transverse mass kink*, *JHEP* **0802** (2008) 035, [[arXiv:0711.4526](#)].
 - [94] **CMS Collaboration** Collaboration, G. Bayatian et al., *CMS technical design report, volume II: Physics performance*, *J.Phys.* **G34** (2007) 995–1579. <http://cds.cern.ch/record/942733/files/lhcc-2006-021.pdf>.
 - [95] **ATLAS Collaboration** Collaboration, N. Rompotis, *Beyond Standard Model Higgs boson physics with ATLAS*, .
 - [96] A. Belyaev, N. D. Christensen, and A. Pukhov, *CalcHEP 3.4 for collider physics within and beyond the Standard Model*, *Comput.Phys.Commun.* **184** (2013) 1729–1769, [[arXiv:1207.6082](#)].
 - [97] G. Belanger, F. Boudjema, P. Brun, A. Pukhov, S. Rosier-Lees, et al., *Indirect search for*

dark matter with micrOMEGAs2.4, *Comput.Phys.Commun.* **182** (2011) 842–856, [[arXiv:1004.1092](#)].

- [98] **Planck Collaboration** Collaboration, P. Ade et al., *Planck 2013 results. XVI. Cosmological parameters*, *Astron.Astrophys.* **571** (2014) A16, [[arXiv:1303.5076](#)].
- [99] T. Li and Y.-F. Zhou, *Strongly first order phase transition in the singlet fermionic dark matter model after LUX*, *JHEP* **1407** (2014) 006, [[arXiv:1402.3087](#)].
- [100] D. G. Cerdeno and A. M. Green, *Direct detection of WIMPs*, [arXiv:1002.1912](#).
- [101] **LUX Collaboration** Collaboration, D. Akerib et al., *First results from the LUX dark matter experiment at the Sanford Underground Research Facility*, *Phys.Rev.Lett.* **112** (2014) 091303, [[arXiv:1310.8214](#)].
- [102] **XENON1T collaboration** Collaboration, E. Aprile, *The XENON1T Dark Matter Search Experiment*, [arXiv:1206.6288](#).
- [103] S. Dawson, A. Gritsan, H. Logan, J. Qian, C. Tully, et al., *Higgs Working Group Report of the Snowmass 2013 Community Planning Study*, [arXiv:1310.8361](#).
- [104] M. E. Peskin, *Estimation of LHC and ILC Capabilities for Precision Higgs Boson Coupling Measurements*, [arXiv:1312.4974](#).
- [105] T. Robens and T. Stefaniak, *Status of the Higgs Singlet Extension of the Standard Model after LHC Run 1*, [arXiv:1501.02234](#).